DOI:
10.1038/s41586-022-05204-z

Document Version
Peer reviewed version

CDK11 regulates pre-mRNA splicing by phosphorylation of SF3B1

Milan Hluchý[1,*], Pavla Gajdušková[1,*], Igor Ruiz de Los Mozos[2-4], Michal Rájecký[1], Michael Kluge[5], Benedict-Tilman Berger[7,8], Zuzana Slabá[1], David Potěšil[1], Elena Weiß[5], Jernej Ule[2,6], Zbyněk Zdráhal[1], Stefan Knapp[7,8], Kamil Paruch[9,10], Caroline C. Friedel[5], Dalibor Blazek[1,11]

[1]Central European Institute of Technology (CEITEC), Masaryk University, 62500 Brno, Czech Republic

[2]The Francis Crick Institute, London, UK

[3]Department of Personalized Medicine, NASERTIC, Government of Navarra, Pamplona, Spain

[4]Center for Applied Medical Research, University of Navarra, Pamplona, Spain

[5]Institut für Informatik, Ludwig-Maximilians-Universität München, München, Germany.

[6]UK Dementia Research Institute Centre at King's College London, London, UK

[7]Structural Genomics Consortium (SGC), Buchmann Institute for Life Sciences (BMLS), Goethe University Frankfurt am Main, Max-von-Laue-Str. 15, 60438 Frankfurt am Main, Germany

[8]Institut für Pharmazeutische Chemie, Goethe University Frankfurt am Main, Max-von-Laue-Str. 9, Frankfurt am Main 60438, Germany.

[9]Department of Chemistry, Faculty of Science, Masaryk University, Kamenice 5/A8, 625 00 Brno, Czech Republic.

[10]International Clinical Research Center, St. Anne's University Hospital in Brno, 602 00 Brno, Czech Republic

[*]These authors contributed equally to this publication

[11]Corresponding author: dalibor.blazek@ceitec.muni.cz

Contact: Dalibor Blazek, PhD. E-mail: dalibor.blazek@ceitec.muni.cz

Abstract

RNA splicing, the process of intron removal from pre-mRNA, is essential for the regulation of gene expression. It is controlled by the spliceosome, a megadalton RNA-protein complex that assembles de novo on each pre-mRNA intron via an ordered assembly of intermediate complexes[1,2]. Spliceosome activation is a major control step requiring dramatic protein and RNA rearrangements leading to a catalytically active complex[1-5]. Splicing factor 3B subunit 1 (SF3B1) protein, a subunit of the U2 snRNP[6], is phosphorylated during spliceosome activation[7-10], but the responsible kinase has not been identified. Here we show that cyclin-dependent kinase 11 (CDK11) associates with SF3B1 and phosphorylates threonine residues at its N-terminus during spliceosome activation. The phosphorylation is important for association of SF3B1 with U5 and U6 snRNAs in activated spliceosome, termed B^{act} complex, and it can be blocked by OTS964, a potent and selective inhibitor of CDK11. CDK11 inhibition prevents spliceosomal transition from the precatalytic complex B to the activated complex B^{act} and leads to widespread intron retention and accumulation of non-functional spliceosomes on pre-mRNAs and chromatin. We demonstrate a central role of CDK11 in spliceosome assembly and splicing regulation and characterize OTS964 as a highly selective CDK11 inhibitor that suppresses spliceosome activation and splicing.

Introduction

Intermediate spliceosome complexes A, B, B^{act}, B*, C and C* are formed by stepwise recruitment and release of five ribonucleoprotein particles (snRNPs) called U1, U2, U4, U5 and U6 and many non-snRNP proteins[1]. Recruitment of U2 snRNP to the intron branch point (BP) results in formation of the A complex, which is followed by U4/U6.U5 tri-snRNP recruitment and creation of the B complex[2]. Although it contains all snRNPs, the B complex is still catalytically inactive[3]. During its activation, U1, U4 snRNPs and non-snRNP B-specific proteins are released, and the retention and splicing complex (RES) and intron binding complex (IBC) are recruited leading to the activated B^{act} spliceosome[4,5]. Human SF3B1, part of the U2 snRNP[6], is essential for splicing. Its C-terminal HEAT-repeat domain plays a crucial role in BP recognition and it is targeted by splicing inhibitors including pladienolide B (pladi B)[11,12]. The N-terminal region of SF3B1 contains 28 repeats of threonine-proline rich sequences and several serine residues that may also be phosphorylated[7,13,14]. SF3B1 is phosphorylated during spliceosome activation[7-10] and upon formation of B^{act}, it is present exclusively in its hyperphosphorylated form[8,10] until the second catalytic reaction when SF3B1 is dephosphorylated[7,10,15]. CDK11 has been associated with transcription/mRNA-processing[16-19], and earlier studies have suggested a role in splicing[16,17,20]. CDK11 phosphorylates the C-terminal domain (CTD) of RNA Polymerase II (RNAPII) *in vitro*[18,19,21], but due to the lack of selective CDK11 inhibitors, cellular substrates and functions of CDK11 have not been characterized. However, a recent study has identified OTS964 as a potent CDK11 inhibitor, with 10-fold selectivity over several other CDKs that decreased proliferation of several cancer cell lines in a CDK11-dependent manner[22].

OTS964 is a selective CDK11 inhibitor

To assess kinome-wide selectivity *in vitro,* we profiled OTS964 at 1 μM concentration in a panel of 412 human kinases (Eurofins). Although the panel contained neither CDK11 nor the kinase TOPK (PBK), the originally reported target of OTS964[23], the screen provided information about the selectivity of OTS964 against most cellular kinases. Only 11 kinases, including CDK9, showed more than 50% reduction of the kinase activity (**Fig. 1a, Supplementary Table 1**). Half-inhibitory concentration (IC_{50}) for these 11 kinases and 15 members of the CDK family were below 1 μM only for TYK2 (IC_{50} = 207 nM), PRK1 (IC_{50} = 508 nM) and CDK9 (IC_{50} = 538 nM) (**Supplementary Table 2, Supplementary Data File 1**). An independent *in vitro kinase assay (IVKA)* with CDK9 determined IC_{50} for OTS964 at 1080 nM (**Extended Fig. 1a**). In contrast, OTS964 inhibited CDK11 with IC_{50} values of 10-100 nM using different assay formats (see below), in agreement with the reported K_D value (40 nM)[22]. Thus, OTS964 is a highly selective inhibitor that affects only four off-target kinases *in vitro* with IC_{50} values at or below 1 μM, including TOPK[23] (IC_{50} = 300-350 nM[24]) **(Extended Fig. 1b).** Notably, our biophysical assays did not show any binding of OTS964 to recombinant TOPK **(Extended Fig. 1c, d**), further supporting the previous finding that the primary target of OTS964 is CDK11[22].

To determine concentrations of OTS964 needed for *in vitro* inhibition of CDK11, we performed *IVKA* with recombinant RNAPII CTD[19], CDK11 wild type (WT) and a OTS964-resistant CDK11 G579S[22] mutant and CDK9[25]. While addition of OTS964 inhibited CDK11 at 10 nM, CDK11 G579S efficiently phosphorylated serine 2 (Ser2) and Ser5 at 500 and 1000 nM concentrations, respectively. Importantly, CDK9-mediated phosphorylation was insensitive to all tested OTS964 concentrations (**Fig. 1b)**.

To assess engagement of OTS964 with CDK11 in living cells, we performed NanoBRET assays[26,27]. The 50% decrease of the NanoBRET signal corresponded to 102 nM concentration of OTS964 (**Fig. 1c**), revealing strong inhibitory potency of the compound against CDK11 in living cells. In contrast, analogous decrease of the NanoBRET signal for CDK9 required at least 13-fold higher concentrations of OTS964, strongly suggesting that CDK9 is not a significant off-target of OTS964 in living cells when used at appropriate concentration (**Fig. 1c, Extended Fig. 1e**). Of note, TYK2 did not engage with OTS964 in living cells (**Extended Fig. 1f**).

To elucidate whether the RNAPII CTD phosphorylation is dependent on CDK11 *in vivo,* we incubated HCT116 cells with OTS964. The treatments showed reduction of total CTD phosphorylation of Tyr1, Ser2, Thr4, Ser5 and Ser7 after 2 to 4 h at concentrations of 30 to 100 nM, respectively **(Fig. 1d, Extended Fig. 2a)**. To confirm the selectivity of OTS964 for CDK11 in cells, we treated HCT116 CDK11 WT or G579S cells with either OTS964 or flavopiridol, which inhibits other CTD kinases including CDK9[28,29]. In contrast to OTS964, flavopiridol-mediated decrease in CTD phosphorylation and expression of 14 replication-dependent histone genes were not rescued in cells harboring CDK11 G579S (**Extended Fig. 2b, c, d**). OTS964 also reduced cellular growth and caused accumulation of cells in G2/M phase in the CDK11-dependent manner, as reported[22] (**Extended Fig. 2e, f**). Altogether, these data are consistent with the high potency and selectivity of OTS964 against CDK11 *in vitro* and in cells.

CDK11 inhibition blocks splicing

To investigate how inhibition of CDK11 affects gene expression, we performed RNA-seq on nuclear extracts of cells treated with OTS964. Inhibition by OTS964 resulted in differential expression of 2742 genes ($|\log_2$ fold change$| > 1$, $P<0.01$), of which 1882 and 860 were

downregulated and upregulated, respectively (**Fig. 2a**). Manual inspection of individual genes revealed massive retention of introns in transcripts (**Fig. 2b**, **Extended Fig. 3a**), suggesting global inhibition of splicing.

To rigorously analyze the global splicing defect, the splicing ratio was calculated separately for 5´SS and 3´SS [30] and we observed statistically significant (Wilcoxon signed rank test; $p<2.2.10^{-16}$) accumulation of unspliced reads when all introns were considered (**Fig. 2c**) and also when first, middle, and last introns were analyzed separately (**Extended Fig. 3b**). RT-qPCR showed accumulation of unspliced introns upon OTS964 treatment in CDK11 WT cells. The accumulation was rescued in CDK11 G579S cells, confirming specificity of the splicing defect for CDK11 activity (**Fig. 2d**). In contrast, only a general decrease in expression of transcripts was observed upon the control treatments with flavopiridol (**Extended Fig. 3c**).

To analyze co-transcriptional splicing in nascent RNA, cells were treated with either OTS964 or pladi B[12,30,31]. Nascent RNA was labelled with 4-thiouridine (4SU) for 15 min and either sequenced immediately (pulse) or 2 h after the 4SU removal (chase) with the latter condition reflecting pre-mRNA processing of the transcripts (**Fig. 2e**). To evaluate splicing change, we calculated the intron ratio as the total number of intronic reads divided by the total number of intronic and exonic reads for each gene. This analysis showed a statistically significant (Wilcoxon rank sum test, $p<0.0004$ in all comparisons) increase in intron ratio over all genes for both OTS964 and pladi B (**Extended Fig. 3d**). An alternative analysis which normalizes to the length of introns and exons, showed a ~1.09-fold median increase in intron ratio in pulse and 2.6- (OTS964) and 2.4-fold (pladi B) increases in chase (Wilcoxon rank sum test, $p< 10^{-15)}$ (**Fig. 2f**). Comparable effects of OTS964 and pladi B regarding the increased frequencies of unspliced pre-mRNA over

all genes strongly suggest that CDK11 inhibition affects global splicing (**Fig. 2f, Extended Fig. 3d, e**).

To rigorously compare the effects of OTS964 and pladi B on splicing, we compared intron ratios for each gene between the treatments. We observed small changes in intron ratios already in the pulse experiment for both OTS964 and pladi B, but in chase the effect was substantial (**Fig. 2g, Extended Fig. 3f**). Comparisons of intron ratios between OTS964 and pladi B and $\log_2$ fold changes of the intron ratio between pladi B/DMSO and OTS964/DMSO did not show much difference between individual genes, with just 73 genes being more affected by pladi B (**Fig. 2h, Extended Fig. 3g, h Supplementary Table 3**). Despite these minor differences, we conclude that OTS964 and pladi B affect splicing in a similar way.

CDK11 inhibition affects transcription

Inhibition of splicing affects transcription dynamics and alters RNAPII phosphorylation profiles[30,32,33]. Our analyses of cell lysates treated with pladi B showed a decrease of bulk cellular levels of all tested CTD modifications (**Extended Fig. 4a**). Since OTS964 affected splicing and CTD phosphorylation comparably to pladi B (**Fig. 1d, 2h, Extended Fig. 2a, 3g, 4a**), we carried out ChIP-seq experiments to determine how the occupancy of total RNAPII and its modified forms (P-Ser2, P-Ser5 and P-Ser7) is affected by CDK11 inhibition.

Metagene plots of 7,500 protein-coding genes revealed increased occupancy of RNAPII at the transcription start site (TSS) (**Extended Fig. 4b**), which is consistent with higher promoter-proximal pausing. The same or similar RNAPII profiles were observed when genes were sorted based on gene expression changes in RNA-seq (**Extended Fig. 4c**) or gene length (**Extended Fig. 4d**). Analyses of the pausing index (PI) for 8885 expressed genes revealed an increase for 6371

(72%) and a decrease for 2503 (28%) genes, with genes with decreased PI being less expressed (**Extended Fig. 4e, f, g**). The changes of P-Ser5 and P-Ser7 metagene profiles upon CDK11 inhibition were almost identical to those for RNAPII (**Extended Fig. 4b, h, i**). The elongation-associated P-Ser2 increased on promoters and decreased and shifted downstream at gene 3´ ends, particularly after the transcription termination sites (TTS) (**Extended Fig. 5a**). The altered occupancy profiles were visible in all gene groups irrespective of expression changes or gene length (**Extended Fig. 5b, c)**, suggesting a general rather than gene-specific phenomenon. The genome-wide trends in RNAPII, P-Ser2, P-Ser5 and P-Ser7 occupancies were evident on individual genes (**Extended Fig. 5d**). Altogether, altered occupancies of RNAPII and P-Ser2 suggest that CDK11 inhibition changes transcriptional dynamics likely by affecting promoter-proximal pausing, elongation and termination.

CDK11 binds and phosphorylates SF3B1

To elucidate how CDK11 regulates splicing, we set up *in vitro* splicing assays in HeLa nuclear extract[34]. Comparison of products of splicing reaction upon OTS964 and control pladi B treatments revealed neither spliced mRNAs nor presence of intron lariat **(Fig. 3a),** concluding that OTS964 inhibits splicing prior to the first catalytic step. Analysis of the intermediates of spliceosome assembly in the presence of increasing concentrations of OTS964 revealed accumulation of B complexes starting at concentrations ≥ 200 nM (**Extended Fig. 6a-c**). Analyses of kinetics of spliceosome intermediates and absence of phosphorylated SF3B1 in nuclear extracts in the presence of OTS964 confirmed formation of the stalled and inactive B complex; in contrast, pladi B stalled spliceosome in A-like complex, as expected[30,31] (**Fig. 3b**).

To identify CDK11 interacting factors and candidate substrates, we immunopurified CDK11 from nuclear extracts. Mass spectrometry analyses of associated factors identified proteins SF3B1 and SF3B3 (**Fig. 3c)**. Independent immunoprecipitations of endogenous CDK11 and SF3B1 confirmed their interaction, but no association of SF3B1 with other transcriptional kinases, CDK9[35] or CDK12[36] or with originally reported candidate SF3B1 kinases CDK1 or CDK2[37] (**Fig. 3d, Extended Fig. 7a**). We observed binding between *Escherichia coli*-expressed N-terminal region of SF3B1 and CDK11 purified from HCT116 cells, which is indicative of direct interaction, although the possibility of other factors contributing to the interaction in vivo cannot be excluded (**Extended Fig. 7b**).

To determine whether SF3B1 is a substrate of CDK11, we used analog-sensitive (AS)[38] CDK11 kinase in *IVKA*. Western blotting analyses showed that CDK11 strongly phosphorylated full-length SF3B1 and the threonine-proline-rich region, but not the HEAT-repeat domain (**Extended Fig. 7c, d**). Thr211, Thr235, Thr313 and Thr328 in SF3B1 are phosphorylated in the process of spliceosome activation starting after the B complex assembly[7,9,10]. Strikingly, these modifications were substantially diminished already after 3 min of OTS964 addition to cells. The CDK11-specific effect was confirmed in cells carrying OTS964-resistant mutation or in control cells carrying SF3B1 with pladi B-resistant mutation R1074H[39] (**Fig. 3e, Extended Fig. 7e)**. Mass spectrometry analyses of immunoprecipitated SF3B1 showed that other active spliceosome-linked phosphorylation of Ser and Thr residues[10] was absent upon CDK11 inhibition (**Extended Fig. 7f**). *IVKA* with recombinant N-terminal domain of SF3B1 and phospho-specific antibodies showed that CDK11 WT and CDK11 G579S efficiently phosphorylated SF3B1 Thr residues. Addition of OTS964 inhibited CDK11 WT at concentrations of 100 nM, but blockage of the control drug-resistant mutant CDK11 G579S required higher concentrations (**Fig. 3f**).

Treatment with dinaciclib[40], a potent inhibitor of SF3B1 candidate kinases CDK1/CDK2[37] and CDK9[41], showed reduced phosphorylation only after 1 h of inhibition (**Extended Fig. 7g**). In addition, dinaciclib did not inhibit splicing or assembly of spliceosome intermediates in *in vitro* splicing assays (**Extended Fig. 7h**), indicating that CDK1/CDK2 and CDK9 do not directly target SF3B1 on the inspected Thr residues. Notably, pladi B reduced phosphorylation to undetectable levels after 30 min, with no change observed in control pladi B-resistant cells[39] (**Extended Fig. 8a**). In contrast, the SF3B1-R1074H and CDK11 G579S cell lines were fully sensitive to OTS964 and pladi B, respectively (**Extended Fig. 8b, c**). To compare the dynamics of OTS964 and pladi B on SF3B1-mediated splicing, we treated HCT116 WT, CDK11 G579S and SF3B1 R1074H cell lines either with OTS964 or pladi B and measured splicing of endogenous *Riok3* and *Ccnl1* genes. The splicing dynamics were similar for both compounds on both genes. Both drug-resistant mutations efficiently blocked the effect of the respective compound and allowed the other compound to fully induce the splicing defect (**Extended Fig. 8d, e**), confirming the compound-specific outcome of the observed splicing defects and further supporting the concept that OTS964 and pladi B work by different mechanisms despite their similar outcome on pre-mRNA splicing (**Fig. 2, 3**). CDK11 potentially binds SR proteins[17,42]; however, western blot analyses of OTS964-treated cell lysates with pan-phospho-RS-specific antibody did not reveal any reduction in phosphorylation (**Extended Fig. 8f**).

B to B^{act} transition is CDK11-regulated

To investigate how CDK11 inhibition affects spliceosome assembly, we performed iCLIP (individual-nucleotide resolution Cross-Linking and ImmunoPrecipitation) with RNA-binding components of the spliceosome (U2AF[65], SF3B1, AQR) as proxies for binding of various

spliceosomal complexes on pre-mRNA. Treatment with OTS964 or pladi B did not affect the general ability of U2AF^{65} or SF3B1 to bind RNA, but some decrease was observed for AQR upon the OTS964 treatment (**Extended Fig. 9a-c, Supplementary Table 4**). For genome-wide analyses we combined replicates (**Extended Fig. 9d**), which demonstrated the largest proportion of binding on intronic RNA (**Extended Fig. 9e, f, g**), with strongest enrichment just upstream of 3´SS, as expected (**Fig. 4a-c**)[43-45]. Metagene analyses of U2AF^{65} binding revealed its increased occupancy after treatments with both OTS964 and pladi B, consistent with a block of the spliceosome in B- and A-like complexes, respectively (**Fig. 3b**, **4a**). In contrast, SF3B1 increased occupancy on pre-mRNA only after the treatment with OTS964, consistent with our observation that OTS964 causes stalling of spliceosome assembly at a later spliceosome intermediate (**Fig. 3b, 4b**). iCLIP with IBC subunit AQR showed that CDK11 inhibition prevents its association with pre-mRNA (**Fig. 4c**), indicating that CDK11 inhibition stalls spliceosome assembly prior to formation of the B^{act} complex[4]. Inspection of individual genes confirmed our findings from iCLIP metagene analyses (**Fig. 4d, Extended Fig. 9h**).

Since co-transcriptional splicing and spliceosome assembly occur on chromatin[46,47], we isolated insoluble (chromatin) fractions[48] and determined chromatin abundance of U1, U2, U4, U5 and U6 snRNAs as a proxy for spliceosomal complex intermediates. Treatment with pladi B caused increased chromatin association of U1, some decrease for U2, and more reduction for U4, U5 and U6, a result consistent with formation of A-like complexes. OTS964 treatment led to increased association of all snRNAs on chromatin, most dramatic for U4 snRNA, suggesting that fully assembled spliceosome in the B complex (i.e., prior to eviction of U4) is the endpoint of CDK11 inhibition and the result is CDK11-specific (**Fig. 4e, f**). This was confirmed by western blotting analyses of proteins specific for U1-U6 snRNPs (i.e., U1 (70K-U1), U2 (SF3B1), U5

(SNU114), U4/U6 (SNU13)) showing slight increase for 70K-U1, SF3B1, and SNU13 or little change for SNU114. In contrast, the pladi B treatment led to diminished association of all the proteins with chromatin with the exception of 70K-U1 (**Fig. 4g, upper panels**). To obtain more detailed insight into the composition of spliceosome B complex intermediate, we performed western blotting analyses with proteins specific for complexes recruited during spliceosome activation, i.e., complex of B-specific proteins (SMU1, MFAP1), RES complex (SNIP1) and IBC complex (AQR). After CDK11 inhibition, the levels of SMU1 and MFAP1 did not change or slightly increased on chromatin, but SNIP1 and AQR were diminished (**Fig. 4g, middle panels**). The defect in SNIP1 and AQR incorporation was rescued in OTS964-resistant cells (**Extended Fig. 9i**). This suggests that the spliceosome assembly was stopped at the stage of a B complex intermediate when B-specific proteins are already present and B^{act}-specific complexes RES and IBC are not yet recruited[4]. The control treatment with pladi B led to diminished presence of SMU1, MFAP1, SNIP1 and AQR on chromatin (**Fig. 4g, middle panels**) and optimal fractionation and effect of both compounds were verified (**Fig. 4g, Extended Fig. 9i, lower panels**).

Finally, we used RNA immunoprecipitation (RIP) of total and phosphorylated (P-Thr235) SF3B1 from the chromatin fractions to study their interactions with U1-U6 snRNAs with qPCR. This revealed the P-Thr235-SF3B1 ±7-14-fold enriched on U5 and U6 as compared to total SF3B1, and this enrichment was lost upon CDK11 inhibition with OTS964 (**Extended Fig. 10a, b, c).** Interestingly, the total SF3B1 was >2-fold enriched on U2 and U4 compared to P-Thr235-SF3B1, and neither phosphorylated nor total SF3B1 had any interaction with U1 snRNAs, as expected. These results indicate that CDK11 is essential for the phosphorylation of SF3B1 that enables interactions with U5 and U6 snRNAs in the activated B^{act} spliceosome intermediate and their engagement in the splicing process.

Discussion

We characterized OTS964 as a highly selective CDK11 inhibitor that blocks pre-mRNA splicing and spliceosomal transition from the B to B^{act} complex. Moreover, we demonstrated that CDK11 associates with SF3B1 and phosphorylates its threonine residues during spliceosome activation (**Extended Fig. 10d)**.

Identification of SF3B1 as a substrate of CDK11 phosphorylation points to a direct role of CDK11 in the regulation of co-transcriptional splicing and spliceosome assembly. Although CDK11 was found in several earlier studies in various spliceosome complexes[49,50], its interacting proteins, substrates and function in splicing remained largely unexplored. By using a selective CDK11 inhibitor, OTS964, we demonstrate that CDK11 activity is needed for phosphorylation of key threonine residues of SF3B1 that are being phosphorylated during spliceosome activation. Strikingly, OTS964 leads to decreased SF3B1 phosphorylation as rapidly as 3 min after addition of this inhibitor. This suggests not only that CDK11 is a bona fide SF3B1-phosphorylating kinase, but also implies rapid interplay between phosphorylation and dephosphorylation of these residues and an important regulatory role of CDK11 in the regulation of splicing. Alike to splicing inhibition with pladi B, OTS964 affects transcription dynamics and causes relatively unspecific phosphorylation decrease of all individual RNAPII CTD residues (**Extended Fig. 10e)**. These observations support the concept that efficient RNAPII transcription requires co-transcriptional assembly of functional spliceosomes[30]. This, however, does not exclude the possibility that CDK11 kinase has a direct role in the regulation of transcription, including direct phosphorylation of some residues in the CTD. We anticipate that future studies will address these scenarios and

determine further roles of CDK11 in the regulation of splicing and transcription using the highly selective chemical probe OTS964 for this kinase, as well as explore the therapeutic potential of splicing modulation via CDK11 inhibition.

Main Text References

1. Wilkinson, M.E., Charenton, C. & Nagai, K. RNA Splicing by the Spliceosome. *Annu Rev Biochem* **89**, 359-388 (2020).
2. Wahl, M.C., Will, C.L. & Luhrmann, R. The spliceosome: design principles of a dynamic RNP machine. *Cell* **136**, 701-718 (2009).
3. Bertram, K.*, et al.* Cryo-EM Structure of a Pre-catalytic Human Spliceosome Primed for Activation. *Cell* **170**, 701-713 e711 (2017).
4. Townsend, C.*, et al.* Mechanism of protein-guided folding of the active site U2/U6 RNA during spliceosome activation. *Science* **370**(2020).
5. Zhang, X.*, et al.* Structure of the human activated spliceosome in three conformational states. *Cell Res* **28**, 307-322 (2018).
6. Sun, C. The SF3b complex: splicing and beyond. *Cell Mol Life Sci* **77**, 3583-3595 (2020).
7. Wang, C.*, et al.* Phosphorylation of spliceosomal protein SAP 155 coupled with splicing catalysis. *Genes & development* **12**, 1409-1414 (1998).
8. Agafonov, D.E.*, et al.* Semiquantitative proteomic analysis of the human spliceosome via a novel two-dimensional gel electrophoresis method. *Molecular and cellular biology* **31**, 2667-2682 (2011).
9. Bessonov, S.*, et al.* Characterization of purified human Bact spliceosomal complexes reveals compositional and morphological changes during spliceosome activation and first step catalysis. *RNA* **16**, 2384-2403 (2010).
10. Girard, C.*, et al.* Post-transcriptional spliceosomes are retained in nuclear speckles until splicing completion. *Nature communications* **3**, 994 (2012).
11. Schneider-Poetsch, T., Chhipi-Shrestha, J.K. & Yoshida, M. Splicing modulators: on the way from nature to clinic. *J Antibiot (Tokyo)* (2021).
12. Kotake, Y.*, et al.* Splicing factor SF3b as a target of the antitumor natural product pladienolide. *Nat Chem Biol* **3**, 570-575 (2007).
13. Thickman, K.R., Swenson, M.C., Kabogo, J.M., Gryczynski, Z. & Kielkopf, C.L. Multiple U2AF65 binding sites within SF3b155: thermodynamic and spectroscopic characterization of protein-protein interactions among pre-mRNA splicing factors. *J Mol Biol* **356**, 664-683 (2006).
14. Murthy, T.*, et al.* Cyclin-dependent kinase 1 (CDK1) and CDK2 have opposing roles in regulating interactions of splicing factor 3B1 with chromatin. *The Journal of biological chemistry* **293**, 10220-10234 (2018).
15. Shi, Y., Reddy, B. & Manley, J.L. PP1/PP2A phosphatases are required for the second step of Pre-mRNA splicing and target specific snRNP proteins. *Molecular cell* **23**, 819-829 (2006).

16. Loyer, P., *et al.* The RNA binding motif protein 15B (RBM15B/OTT3) is a functional competitor of serine-arginine (SR) proteins and antagonizes the positive effect of the CDK11p110-cyclin L2alpha complex on splicing. *The Journal of biological chemistry* **286**, 147-159 (2011).
17. Hu, D., Mayeda, A., Trembley, J.H., Lahti, J.M. & Kidd, V.J. CDK11 complexes promote pre-mRNA splicing. *The Journal of biological chemistry* **278**, 8623-8629 (2003).
18. Pak, V., *et al.* CDK11 in TREX/THOC Regulates HIV mRNA 3' End Processing. *Cell Host Microbe* **18**, 560-570 (2015).
19. Gajduskova, P., *et al.* CDK11 is required for transcription of replication-dependent histone genes. *Nature structural & molecular biology* **27**, 500-510 (2020).
20. Loyer, P., *et al.* Characterization of cyclin L1 and L2 interactions with CDK11 and splicing factors: influence of cyclin L isoforms on splice site selection. *The Journal of biological chemistry* **283**, 7721-7732 (2008).
21. Trembley, J.H., Hu, D., Slaughter, C.A., Lahti, J.M. & Kidd, V.J. Casein kinase 2 interacts with cyclin-dependent kinase 11 (CDK11) in vivo and phosphorylates both the RNA polymerase II carboxyl-terminal domain and CDK11 in vitro. *The Journal of biological chemistry* **278**, 2265-2270 (2003).
22. Lin, A., *et al.* Off-target toxicity is a common mechanism of action of cancer drugs undergoing clinical trials. *Sci Transl Med* **11**(2019).
23. Matsuo, Y., *et al.* TOPK inhibitor induces complete tumor regression in xenograft models of human cancer through inhibition of cytokinesis. *Sci Transl Med* **6**, 259ra145 (2014).
24. Hu, Q.F., *et al.* Design, synthesis and biological evaluation of novel 1-phenyl phenanthridin-6(5H)-one derivatives as anti-tumor agents targeting TOPK. *Eur J Med Chem* **162**, 407-422 (2019).
25. Czudnochowski, N., Bosken, C.A. & Geyer, M. Serine-7 but not serine-5 phosphorylation primes RNA polymerase II CTD for P-TEFb recognition. *Nature communications* **3**, 842 (2012).
26. Vasta, J.D., *et al.* Quantitative, Wide-Spectrum Kinase Profiling in Live Cells for Assessing the Effect of Cellular ATP on Target Engagement. *Cell Chem Biol* **25**, 206-214 e211 (2018).
27. Wells, C.I., *et al.* Quantifying CDK inhibitor selectivity in live cells. *Nature communications* **11**, 2743 (2020).
28. Chao, S.H. & Price, D.H. Flavopiridol inactivates P-TEFb and blocks most RNA polymerase II transcription in vivo. *The Journal of biological chemistry* **276**, 31793-31799 (2001).
29. Greifenberg, A.K., *et al.* Structural and Functional Analysis of the Cdk13/Cyclin K Complex. *Cell reports* **14**, 320-331 (2016).
30. Caizzi, L., *et al.* Efficient RNA polymerase II pause release requires U2 snRNP function. *Molecular cell* **81**, 1920-1934 e1929 (2021).
31. Effenberger, K.A., *et al.* Coherence between cellular responses and in vitro splicing inhibition for the anti-tumor drug pladienolide B and its analogs. *The Journal of biological chemistry* **289**, 1938-1947 (2014).
32. Koga, M., Hayashi, M. & Kaida, D. Splicing inhibition decreases phosphorylation level of Ser2 in Pol II CTD. *Nucleic acids research* **43**, 8258-8267 (2015).
33. Nojima, T., *et al.* Mammalian NET-Seq Reveals Genome-wide Nascent Transcription Coupled to RNA Processing. *Cell* **161**, 526-540 (2015).

34. Luo, M.J. & Reed, R. Splicing is required for rapid and efficient mRNA export in metazoans. *Proceedings of the National Academy of Sciences of the United States of America* **96**, 14937-14942 (1999).
35. AJ, C.Q., Bugai, A. & Barboric, M. Cracking the control of RNA polymerase II elongation by 7SK snRNP and P-TEFb. *Nucleic acids research* **44**, 7527-7539 (2016).
36. Pilarova, K., Herudek, J. & Blazek, D. CDK12: cellular functions and therapeutic potential of versatile player in cancer. *NAR Cancer* **2**, zcaa003 (2020).
37. Seghezzi, W., *et al.* Cyclin E associates with components of the pre-mRNA splicing machinery in mammalian cells. *Molecular and cellular biology* **18**, 4526-4536 (1998).
38. Lopez, M.S., Kliegman, J.I. & Shokat, K.M. The logic and design of analog-sensitive kinases and their small molecule inhibitors. *Methods Enzymol* **548**, 189-213 (2014).
39. Yokoi, A., *et al.* Biological validation that SF3b is a target of the antitumor macrolide pladienolide. *FEBS J* **278**, 4870-4880 (2011).
40. Paruch, K., *et al.* Discovery of Dinaciclib (SCH 727965): A Potent and Selective Inhibitor of Cyclin-Dependent Kinases. *ACS Med Chem Lett* **1**, 204-208 (2010).
41. Sanso, M., *et al.* P-TEFb regulation of transcription termination factor Xrn2 revealed by a chemical genetic screen for Cdk9 substrates. *Genes & development* **30**, 117-131 (2016).
42. Loyer, P., Trembley, J.H., Lahti, J.M. & Kidd, V.J. The RNP protein, RNPS1, associates with specific isoforms of the p34cdc2-related PITSLRE protein kinase in vivo. *Journal of cell science* **111 (Pt 11)**, 1495-1506 (1998).
43. Zarnack, K., *et al.* Direct competition between hnRNP C and U2AF65 protects the transcriptome from the exonization of Alu elements. *Cell* **152**, 453-466 (2013).
44. Briese, M., *et al.* A systems view of spliceosomal assembly and branchpoints with iCLIP. *Nature structural & molecular biology* **26**, 930-940 (2019).
45. Van Nostrand, E.L., *et al.* Principles of RNA processing from analysis of enhanced CLIP maps for 150 RNA binding proteins. *Genome biology* **21**, 90 (2020).
46. Kfir, N., *et al.* SF3B1 association with chromatin determines splicing outcomes. *Cell reports* **11**, 618-629 (2015).
47. Carrocci, T.J. & Neugebauer, K.M. Pre-mRNA Splicing in the Nuclear Landscape. *Cold Spring Harb Symp Quant Biol* **84**, 11-20 (2019).
48. Tresini, M., *et al.* The core spliceosome as target and effector of non-canonical ATM signalling. *Nature* **523**, 53-58 (2015).
49. Deckert, J., *et al.* Protein composition and electron microscopy structure of affinity-purified human spliceosomal B complexes isolated under physiological conditions. *Molecular and cellular biology* **26**, 5528-5543 (2006).
50. Makarov, E.M., *et al.* Small nuclear ribonucleoprotein remodeling during catalytic activation of the spliceosome. *Science* **298**, 2205-2208 (2002).

Main Figure Legend

Fig. 1 OTS964 is a highly selective CDK11 inhibitor

a, Kinome tree representation of selectivity of OTS964 (at 1 μM concentration) in the Eurofins panel of 412 human kinases. The size of red circles depicts % of inhibition of kinase activity. The green circle corresponds to CDK11; the % of CDK11 inhibition was derived from *IVKAs* presented in **Fig. 1b** and **3f**. The blue circle corresponds to TOPK; the % of TOPK inhibition is estimated from the published IC_{50} = 353 nM [24] and **Extended Fig. 1b**.

b, Immunoblots of *IVKA* with flag(F)-tagged-CDK11 WT, G579S and kinase dead (KD) mutants or F-CDK9 WT and KD mutant on glutathione-S-transferase(GST)-tagged-CTD substrate with indicated concentrations of OTS964.

c, Graphs show percentage of normalized NanoBRET ratio for CDK11/Cyclin L2 or CDK9/CyclinT1 upon OTS964 or control dinaciclib treatments. n=2 biologically independent replicates, a representative replicate is shown.

d, Immunoblot of proteins after treatment of cells with OTS964 for 4 h. Short; long=short/long exposures of film. P-RNAPII=phosphorylated RNAPII.

Fig. 2 CDK11 kinase activity is needed for efficient pre-mRNA splicing

a, Volcano plot of differentially expressed genes from nuclear RNA-seq in HCT116 cells treated with 30 nM OTS964 for 4 h. Down- and upregulated genes are in red and blue, respectively.

b, IGV genome browser view of *Wee1* gene from RNA-seq.

c, Box plots showing ratio of spliced reads over total unspliced and spliced reads in RNA-seq. All introns in selected 6222 isoforms were considered. Boxes represent the range between the first and third quartiles for each condition. Black horizontal lines in boxes show the median. The ends of the whiskers extend the box by 1.5 times the inter-quartile range. n=2 biologically independent experiments.

d, Graph shows change in expression of transcripts of five genes in WT or CDK11 G579S HCT116 cells either treated with DMSO or with 50 nM OTS964 for 4 h. mRNA levels were normalized to *Ppia* mRNA and expression in DMSO was set as 1. n=4 biologically independent experiments, error bars=SEM. E-E; E-In=primers spanning exon-exon and exon-intron junctions, respectively.

e, Schema of 4SU-seq experiment.

f, Box plots showing ratio of intronic over exonic read counts per kilobase of length (RPK) in 4SU-seq in pulse (left) or chase (right). Boxes represent the range between the first and third quartiles for each condition. Black horizontal lines in boxes show the median. The ends of the whiskers extend the box by 1.5 times the inter-quartile range. Two biological replicates (REP1 and REP2) are shown.

g, Scatterplots show comparison of intron ratios in individual genes between DMSO and either OTS964 (left) or pladi B (right) treated cells in 4SU-seq chase.

h, Scatterplot comparing $\log_2$ fold changes of intron ratios for individual genes in pladi B/DMSO and OTS964/DMSO in 4SU-seq chase. Differentially affected genes are circled.

Fig. 3 CDK11 phosphorylates SF3B1 on threonine residues required for spliceosome activation

a, Denaturing gel analyses of the radiolabeled *AdML* pre-mRNA and spliced products from *in vitro* splicing reactions in HeLa nuclear extracts upon indicated treatments. Schemes of intron lariat, unspliced substrate, spliced product and intron (from top to bottom) are depicted on the left. -ATP = ATP-depleted nuclear extracts. M=marker.

b, Native gel analyses of kinetics of spliceosome assembly on radiolabeled *AdML* pre-mRNA in HeLa nuclear extracts upon indicated treatments. Identities of spliceosome complexes E, A, B and

C are shown. -ATP = ATP-depleted nuclear extracts (upper panel). Immunoblot of proteins after indicated treatments of the Hela nuclear extracts (lower panel).

c, Silver-stained SDS-PAGE gel showing immunoprecipitates of Flag-tagged empty vector (F-EV) and F-CDK11 with or without RNase A treatment. Identity of specific bands is marked.

d, Immunoblot analyses of immunoprecipitations of endogenous SF3B1. IgG=antibody control.

e, Immunoblot of proteins after treatment of WT or CDK11 G579S HCT116 cells with OTS964.

f, Immunoblots of *IVKA* with F-CDK11 WT, and G579S and KD mutants on GST-SF3B1(1-463) substrate with indicated concentrations of OTS964.

Fig. 4 CDK11 inhibition prevents transition of spliceosome from B to B^{act} complex

a, b, c, Metagene analyses and heatmaps of $U2AF^{65}$ **(a)**, SF3B1 **(b)** and AQR **(c)** iCLIP binding at all 3′SS upon indicated 1 h treatments. BP=branch point. n=2 biologically independent experiments.

d, IGV genome browser view of SF3B1, $U2AF^{65}$ and AQR iCLIP binding at *Ddx47* transcript.

e, f, RT-qPCR analyses of chromatin association of U1, U2, U4, U5 and U6 snRNAs upon indicated 2 h treatments of HCT116 (WT) **(e)** or HCT116 CDK11 G579S **(f)** cells. Chromatin association in DMSO was set as 1; n=4 biologically independent experiments, error bars=SEM.

g, Immunoblot analyses of association of indicated splicing factors in nucleoplasmic (soluble) and chromatin (chrom) fractions upon indicated treatments. Presence of the factors in specific spliceosome complexes is indicated on the right. P indicates phosphorylated forms of RNAPII and SF3B1. Short; long=short/long exposures of film.

Methods

Antibodies

List of antibodies used in the study is provided in **Supplementary Table 5.**

Primers

List of primers used in the study is provided in **Supplementary Table 6.**

Plasmids

List of plasmids used in the study is provided in **Supplementary Table. 7**. Plasmids containing human CDK11 (GenBank accession no. AAC72077) were described previously [19]. The plasmid resulting in G579S mutation in human CDK11 was prepared using QuikChange II XL Site-Directed Mutagenesis Kit (Agilent, no. 200522) according to the manufacturer's protocol.

Plasmid pcDNA3.1-FLAG-SF3B1-WT was a gift from Manoj Pillai (Addgene plasmid # 82576; http://n2t.net/addgene:82576 ; RRID:Addgene_82576). The SF3B1 cDNA was sub-cloned either into pcDNA5/FRT/TO plasmid (Thermo Fisher Scientific) using HindIII and XhoI restriction sites and in frame with 5'3xFlag tag or into bacterial expression vector pGEX-4T-3 (Cytiva, GE28-9545-52) using EcoRI and NotI restriction sites in frame with 5'GST. SF3B1 deletion mutants were sub-cloned into HindIII and XhoI restriction sites of pcDNA5/FRT/TO plasmid (Thermo Fisher Scientific) in frame with 5'3xFlag tag. Primers used for the cloning are specified in **Supplementary Table 6.**

Reagents

List of reagents used in the study is specified in **Supplementary Table 8.**

Cell culture

Human colorectal HCT116 Flp-in cell line (a gift from B. G. Wouters), HEK293 Flp-in cell line (Thermo Fisher Scientific, R75007) and HCT116 cell line (ATCC) were all maintained in DMEM/high-glucose medium supplemented with L-glutamine, sodium pyruvate and 5% FBS at 37 °C and 5% CO_2. The cell lines were not tested for Mycoplasma contamination and were not authenticated.

To prepare cell line stably expressing SF3B1 protein, HEK293 Flp-in cells were transfected with corresponding 3xFlag-tagged SF3B1 plasmid. Resistant colonies were selected with 100 μg/ml of hygromycin (Thermo Fisher Scientific, 10687-010) and two weeks later, individual clones were expanded. Expression of Flag-tagged SF3B1 was induced with 1 μg/ml of doxycycline (Sigma, D3072) and verified by western blotting (Flag, Sigma F3165, 1:3000; SF3B1, MBL MB-D221-3, 1:2000). Flag-tagged SF3B1 protein expression levels were always lower than or equal to expression of endogenous SF3B1.

Unless stated otherwise, for western blot analyses HCT116, HCT116 CDK11 G579S and HCT116 SF3B1 R1074H cells were plated onto 6-well plate to reach 80 % confluency at the day of experiment. The cells were treated with DMSO, 50 nM OTS964, 186 nM pladi B or 20 nM dinaciclib for indicated times. The cells were placed on ice, scraped, washed once with ice-cold PBS and lysed for 10 min in 100 μl of RIPA buffer (50 mM Tris-HCl (pH = 8), 150 mM NaCl, 1 % NP-40, 0.5 % sodium deoxycholate, 0.1 % SDS, 5 mM EDTA, protease inhibitor cocktail (1 μl/ml, Sigma-Aldrich, P8340)). Phosphatase inhibitor cocktail 3 (10 μl/ml, Sigma-Aldrich, P0044) was added in RIPA buffers for experiments detecting SF3B1 phosphorylation and omitted in experiments detecting RNAPII CTD phosphorylation. Protein extracts were clarified by centrifugation at 10,000g for 10 min, 4 °C. Protein concentration in cleared extracts was

560 determined by Pierce™ BCA Protein Assay Kit and equalized into 70 µl using RIPA buffer.
561 Proteins were denatured by addition of 35 µl of 3x Laemmli buffer and boiled for 5 min and
562 resolved by SDS-PAGE. The following antibodies were used for detection: RNAPII (Cell
563 Signaling #14958, 1:1000), Phospho-Ser2 (Chromotek 3E10, 1:500), Phospho-Ser5 (Chromotek
564 3E8, 1:500), Phospho-Ser7 (Chromotek 4E12, 1:1000), Phospho-Tyr1 (Active Motif 61383,
565 1:1000), Phospho-Thr4 (Active Motif 61361, 1:1000), α-Tubulin (Santa Cruz sc-5286, 1:200),
566 SF3B1 (MBL MB-D221-3, 1:2000), FUS (Santa Cruz sc-47711, 1:10000) SF3B1 P-T313 (Cell
567 Signaling 25009S, 1:2000), SF3B1 P-T211 (rabbit antiserum, 1:1000), SF3B1 P-T235 (rabbit
568 antiserum, 1:1000), SF3B1 P-T328 (rabbit antiserum, 1:500) and Pan-P-RS (Sigma MABE50,
569 1:1000).
570
571 **Immunoprecipitation of endogenous proteins**
572 HEK293 cells were plated onto 150-cm^2 plate to reach 90% confluency at the day of experiment.
573 Cells from two plates per condition were scraped and pooled, washed once with PBS, and lysed in
574 3 ml of buffer A (20 mM HEPES-KOH (pH = 7.3), 0.5 % Triton-100, 150 mM KCl, protease
575 inhibitor cocktail (1 µl/ml, Sigma-Aldrich, P8340)) for 10 min. During cell lysis, extracts were
576 sonicated (3 × 5 s, amp 0.30, using 5/64 probe, QSonica Q55A). Protein extracts were clarified by
577 centrifugation at 10,000 g for 10 min, 4 °C. For immunoprecipitations of endogenous proteins,
578 protein G Dynabeads were used; 15 µl of the Dynabeads per immunoprecipitation were washed 3
579 times with 1 ml buffer A. Dynabeads were then incubated in buffer A with 3 µg of SF3B1 (MBL
580 MB-D221-3), 3 µg of CDK11 (abcam ab19393) or 3 µg of IGG control antibodies (Proteintech
581 66360-2-Ig, 30000-0-AP) at 4 °C for 3 h. Clarified cell extracts (10,000 g for 10 min) were then
582 rotated with antibody-coated Dynabeads for 2 h at 4 °C, and were subsequently washed 3 times

with 1 ml of buffer A. Proteins were eluted by addition of 55 µl of 3× Laemmli buffer and being boiled for 5 min. After SDS-PAGE, the following antibodies were used for detection: SF3B1 (MBL MB-D221-3, 1:2000), CDK11 (rabbit antiserum, 1:3000), SF3B4 (Bethyl A303-950A, 1:2000), CDK12 (Santa Cruz sc-81834, 1:1000), CDK9 (Santa Cruz sc-484, 1:1000), CDK1 (Cell Signaling 77055S, 1:500), CDK2 (Santa Cruz sc-163, 1:1000) and CK2a (BD Biosciences 611610, 1:2000).

In vitro splicing assay

Plasmid pSP72-AdML (gift from Robin Reed, Harvard University) was linearized by BamHI digestion and purified from agarose gel. Uniformly [^{32}P]-labeled AdML pre-mRNA was synthesized *in vitro* by MAXIscript™ T7 Transcription Kit (Thermo Fisher, AM1312) using [α-^{32}P]-UTP (Hartmann Analytic, FP-210), purified from 15% acrylamide gel containing 6 M urea and followed by Phenol extraction. Splicing reactions contained 40% HeLa nuclear extract (Ipracell, CC-01-20-005; stock concentration 6 mg/ml in 20 mM HEPES-KOH (pH = 7.9), 100 mM KCl, 0.2 mM EDTA, 20 % glycerol, 0.2 mM PMSF and 0.5 mM DTT) supplemented with KCl to 80 mM final concentration, 1 U of SUPERase•In™ RNase Inhibitor (20 U/µL, Thermo Fisher, AM2694), 3 mM $MgCl_2$, 1 mM ATP, 10 mM creatine phosphate and 4 ng of [^{32}P]-labeled *AdML* pre-mRNA in 20 µl. HeLa nuclear extracts were mixed with DMSO, OTS964 (MedChem Express, HY-12467), pladi B (Cayman Chemical, Cay16538-100), dinaciclib (gift from Kamil Paruch, Masaryk University) or NSC95397 (MedChem Express, HY-108543) and were pre-incubated at 30°C for 15 min. For low $MgCl_2$ control reactions, master mix contained 0.3 mM $MgCl_2$. Splicing reactions were incubated at 30°C for the times indicated. 5 µl of splicing reaction were mixed with 1 µl of 5 mg/ml heparin (Sigma, H3393-100KU) and 1 µl of 6× DNA loading

dye (Thermo Scientific, R0611) and resolved on 2% agarose gel in 0.5× TBE by native gel electrophoresis. Agarose gel was subsequently fixed in fixing solution (10 % acetic acid, 10 % methanol). RNA from the rest of splicing reaction was extracted using Phenol extraction, mixed with Gel Loading Buffer II from MAXIscript™ T7 Transcription Kit (Thermo Fisher, AM1312) and analyzed by denaturing PAGE on 15% acrylamide gel containing 6 M urea in 1× TBE. Low Molecular Weight DNA Ladder (New England Biolabs, N3233S) terminally labeled by T4 polynucleotide kinase (New England Biolabs, M0201S) and [γ-^{32}P]-ATP (Hartmann Analytic, FP-301) was used as a size marker. Both gels were visualized by autoradiography.

In vitro kinase assay with AS CDK11

HEK293 cells were seeded onto 150 cm^2 plates to 60 % confluence and transfected with mammalian expression vectors containing 3xFlag-tagged (F) F-CDK11 AS, F-SF3B1, F-SF3B1 (1-463) and F-SF3B1 (464-1304) constructs using PEI. F-CDK11 AS was co-transfected with Xpress-tagged Cyclin L1. After 48 h the cells were lysed in 1 ml of lysis buffer (20 mM HEPES-KOH (pH = 7.9), 15 % glycerol, 0.2 % NP-40, 150 mM KCl, protease inhibitor cocktail (1 µl/ml, Sigma-Aldrich, P8340)) and the 3xFlag-tagged proteins were immunoprecipitated from cleared lysates with Flag agarose M2 affinity gel (Sigma-Aldrich, A2220). Beads with bound proteins were washed three times with high salt wash buffer (20 mM HEPES-KOH (pH = 7.9), 15 % glycerol, 0.2 % NP-40, 500 mM KCl, protease inhibitor cocktail (1 µl/ml, Sigma-Aldrich, P8340)), once with detergent-free buffer (20 mM HEPES-KOH (pH = 7.9), 15 % glycerol, 150 mM KCl) and 3xFlag-tagged proteins were eluted with 45 µl of Flag elution buffer (20 mM HEPES-KOH (pH = 7.9), 150 mM KCl, 3xFlag peptide (0.2 mg/ml, Sigma-Aldrich, F4799)). For input samples, 5 µl of eluted 3xFlag-tagged proteins were mixed with 5 µl of 3× Laemmli buffer and boiled for

5 min. Each kinase reaction contained 12 µl of eluted 3xFlag-tagged kinase, 20 µl of eluted 3xFlag-tagged substrate (F-SF3B1, F-SF3B1 (1-463) or F-SF3B1 (464-1304)) and kinase buffer (20 mM HEPES-KOH (pH = 7.9), 5 mM $MgCl_2$, protease inhibitor cocktail (1 µl/ml, Sigma-Aldrich, P8340), phosphatase inhibitor cocktail 3 (10 µl/ml, Sigma-Aldrich, P0044) and 833 µM 6-Bn-ATP-γ-S analog (Biolog Life Science Institute, B 072) in total volume 60 µl. Kinase reactions were incubated at 30℃ for 1 h and stopped with addition of 20 mM EDTA. Kinase reactions were alkylated at 4°C overnight with addition of 2 mM p-nitrobenzyl mesylate (Abcam, ab138910), resolved by SDS-PAGE and substrates were detected by western blotting using an anti-thiophosphate ester (TPE) antibody [51]. Inputs were detected by Flag (Sigma F3165, 1:3000), CDK11 (rabbit antiserum, 1:3000) and SF3B1 (MBL MB-D221-3, 1:2000) antibodies.

GST-pulldown

The GST-tagged SF3B1 (1-463) was expressed in BL21 (DE3) pLysS *E. coli* strain using pGEX-4T-3 SF3B1 (1 – 463) plasmid. Cultures were grown in 900 ml of LB medium (supplemented with 100 µg/ml ampicillin and 25 µg/ml chloramphenicol) at 37°C with vigorous shaking to OD_{600} of 0.5. Cultures were induced at 37°C for 16 h in the presence of 0.5 mM isopropyl β-d-1-thiogalactopyranoside (Sigma, I5502). Cells were collected by centrifugation at 5,000 g at 4°C for 10 min. Extracts of cells were prepared by sonication in bacteria lysis buffer (50 mM Tris, 20 % glycerol, 150 mM NaCl, 0.5 mM EDTA, 1 % NP-40, 2 mM PMSF, cOmplete™ Mini Protease Inhibitor Cocktail (1 tablet per 50 ml, Roche, 04693124001)). Lysates were clarified by centrifugation at 10,000 g at 4°C for 10 min, and the resulting supernatant was incubated with 1 ml of Glutathione Sepharose 4B beads (Cytiva, GE17-0756-01) for 1 h at 4°C. The beads were washed with 10 ml of bacteria lysis buffer followed with 40 ml of wash buffer (50 mM Tris, 20 %

glycerol, 200 mM NaCl, 0.5 mM EDTA). GST-tagged SF3B1 (1-463) was eluted eight times with 750 µl of elution buffer (50 mM Tris, 20 % glycerol, 150 mM NaCl, 0.5 mM EDTA, 10 mM glutathione). Fractions containing SF3B1 fragment were pooled together, washed with PBS and concentrated in an Amicon Ultra-4 Centrifugal Filter Unit (Sigma, UFC801024). Samples were stored at –80°C until use.

500 ng of purified GST-tagged SF3B1 (1-463) were incubated with 17 µl of Glutathione Sepharose 4B beads (Cytiva, GE17-0756-01) and F-CDK11 (immunoprecipitated from HCT116 cells) in IP buffer (50 mM Tris, 20 % glycerol, 100 mM KCl, 0.5 mM EDTA, 1 % NP-40, 1 mM DTT). After 30 min incubation on ice with occasional mixing, the samples were centrifuged at 1,000 g at room temperature for 30 s, supernatant was stored and beads were washed 3 times with 100 µl of IP buffer with 300 mM KCl. 30 µl of 3× Laemmli sample buffer was added to the beads and supernatant samples. Samples were boiled at 95°C for 3 min and resolved by SDS-PAGE.

Purification of 3xFlag-tagged SF3B1 and analysis of phosphosites by LC-MS/MS

HEK293 with stably integrated 3xFlag-tagged SF3B1 were seeded onto 150 cm^2 plates to reach 90 % confluence on the day of experiment. Cells were supplemented with fresh medium containing either DMSO or 50 nM OTS964 (MedChem Express, HY-12467). After 1 h, cells from two plates per condition were scraped and pooled, washed once with PBS and lysed in 1 ml of buffer A (20 mM HEPES-KOH (pH = 7.3), 0.5 % Triton-100, 150 mM KCl, protease inhibitor cocktail (1 µl/ml, Sigma-Aldrich, P8340), phosphatase inhibitor cocktail 3 (10 µl/ml, Sigma-Aldrich, P0044)). 3xFlag-tagged SF3B1 was immunoprecipitated from cleared lysates with Flag agarose M2 affinity gel (Sigma-Aldrich, A2220). Beads with bound proteins were washed three times with high salt buffer A (20 mM HEPES-KOH (pH = 7.3), 0.5 % Triton-100, 500 mM KCl, protease inhibitor

cocktail (1 µl/ml, Sigma-Aldrich, P8340), phosphatase inhibitor cocktail 3 (10 µl/ml, Sigma-Aldrich, P0044)) and once with detergent-free buffer (20 mM HEPES-KOH (pH = 7.3), 150 mM KCl). 100 µl of detergent-free buffer was added to the beads with bound proteins and suspension stored at -80°C until processing.

The beads-bound protein complexes were digested directly on beads by addition of 0.75 µg of trypsin (sequencing grade, Promega) in 50 mM $NaHCO_3$ buffer and incubated at 37°C with mild agitation for 2 h. Partially digested complexes were separated from the beads incubated at 37 °C overnight without agitation. Resulting peptides were extracted into new tube by 2.5 % formic acid (FA) in 50 % acetonitrile (ACN) and 100 % ACN and concentrated in a SpeedVac (Thermo Fisher Scientific). The aliquot (1/10) of concentrated sample was transferred to LC-MS vial with already added polyethylene glycol (PEG; final concentration 0.001 % [52], and directly analysed by LC-MS/MS for protein identification. The rest of the sample (9/10) was used for phosphopeptide analysis. Phosphopeptides were enriched using High-Select™ TiO_2 Phosphopeptide Enrichment Kit (Thermo Scientific, Waltham, Massachusetts, USA) according to the manufacturer´s protocol and extracted into LC-MS vial with already added PEG (final concentration 0.001 %). Resulting peptides were analysed by LC-MS/MS.

LC-MS/MS analyses of all peptide mixtures (with and without phosphoenrichment step) were done using nanoElute system (Bruker) connected to timsTOF Pro spectrometer (Bruker). Two column (trapping column: Acclaim™ PepMap™ 100 C18, dimensions 300 µm ID, 5 mm long, 5 µm particles, Thermo Fisher Scientific; separation column: Aurora C18, 75 µm ID, 250 mm long, 1.6 µm particles, Ion Opticks) mode was used on nanoElute system with default equilibration conditions (trap column: 10 volumes at 217.5 bars; separation column: 4 column volumes at 800 bars). Sample loading was done using 3 pickup volumes +2 µl at 100bars. Trapped peptides were

eluted by 60 min linear gradient program (flow rate 400 nl/min, 2-30 % of mobile phase B; mobile phase A: 0.1 % FA in water; mobile phase B: 0.1 % FA in acetonitrile) followed by system wash step at 80 % mobile phase B. The analytical column was placed inside the Column Toaster (40°C; Bruker) and its emitter side was installed into CaptiveSpray ion source (Bruker).

MS data were acquired in the m/z range of 100-1700 and 1/k0 range of 0.6-1.6 $V \times s \times cm^{-2}$ using DDA-PASEF method acquiring 10 PASEF scans with scheduled target intensity of 20,000 and intensity threshold of 2,500. Active exclusion was set for 0.4 min with precursor reconsideration for 4x more intense precursors. Inspect the raw data for more details on the method used.

For data evaluation, we used MaxQuant software (v1.6.17) [53] with inbuild Andromeda search engine [54]. Search was done against protein databases of *UniProtKB Human* (20,609 protein sequences, version from 2020-12-02, downloaded from ftp://ftp.uniprot.org/pub/databases/uniprot/current_release/knowledgebase/reference_proteomes/Eukaryota/UP000005640_9606.fasta.gz) and cRAP contaminants (112 sequences, version from 2018-11-22, downloaded from http://www.thegpm.org/crap). Modifications were set as follows for database search: oxidation (M), deamidation (N, Q), acetylation (Protein N-term) and phosphorylation (S, T, Y) as variable modifications, with carbamidomethylation (C) as a fixed modification. Enzyme specificity was tryptic with two permissible missed cleavages. Only peptides and proteins with false discovery rate threshold ≤ 0.01 were considered. The mass spectrometry proteomics data have been deposited to the ProteomeXchange Consortium[55] and are available via ProteomeXchange dataset PXD035189 (https://doi.org/doi:10.25345/C59P2W974).

NanoBRET target engagement assay

The assay was performed as described previously [26,56]. In brief: Full-length kinase ORF (Promega) cloned in frame with a NanoLuc-vector (as indicated in table below) was transfected into HEK293T cells using FuGENE HD (Promega, E2312) and proteins were allowed to express for 20 h. Serially diluted inhibitor and NanoBRET™ Kinase Tracer (as indicated in the table below) were pipetted into white 384-well plates (Greiner 781 207) using an ECHO 550 acoustic dispenser (Labcyte). The corresponding transfected cells were added and reseeded at a density of 2 x 10^5 cells/ml after trypsinization and resuspension in Opti-MEM without phenol red (Life Technologies). The system was allowed to equilibrate at 37°C for 2 h and 5 % CO_2 prior to BRET measurements. To measure BRET, NanoBRET™ NanoGlo Substrate + Extracellular NanoLuc Inhibitor (Promega, N2160) were added as per the manufacturer's protocol, and filtered luminescence was measured on a PHERAstar plate reader (BMG Labtech) equipped with a luminescence filter pair (450 nm BP filter (donor) and 610 nm LP filter (acceptor)). Competitive displacement data were then plotted using GraphPad Prism 8 software using a normalized 3-parameter curve fit with the following equation: Y=100/(1+10^((X-LogIC50))). Assay conditions used in the NanoBRET target engagement assays are detailed in **Supplementary Table 9.**

RT-PCR

HCT116 WT, HCT116 CDK11 G579S and HCT116 SF3B1 R1074H cells were treated with DMSO, 50 nM OTS964 and 186 nM pladi B for 0.5, 1, 2, or 4 h. Cells were washed twice with ice-cold PBS, scraped, pelleted at 200 g for 3 min and treated for 5 min with 150 µl of cytoplasmic lysis buffer (10 mM Tris-Cl, pH=8, 0.32 M Sucrose, 3 mM $CaCl_2$, 2 mM $MgCl_2$, 0.1 mM EDTA, 0.5 % TritonX-100, supplemented with 40 U/ml RNase inhibitor, Roche, 3335402001). Cytoplasmic RNA present in the supernatant was completely removed after centrifugation (500 g

for 3 min). Nuclear RNA was extracted using Tri-Reagent (93289, Sigma). After DNase treatment (AMPD1, Sigma), 1000 ng of RNA was reverse-transcribed using random hexamers and Superscript II reverse transcriptase (Thermo Fisher). PCR was performed in 20 µl of reaction mixture containing 5 ng of the obtained cDNA (or 50 ng of human genomic DNA as a control), 1x Phusion HF buffer, 0.2 mM dNTP mix, 0.5 µM of each primer and 0.4 U Phusion DNA polymerase (F530S, Thermo Fisher). PCR conditions were 94°C for 30 s; 35 cycles of 94°C for 10 s, 62°C for 20 s, and 72°C for 30 s; followed by 72°C for 10 min. PCR products were separated on a 1.5 % agarose gel and stained with Midori Green (MG03, Nippon Genetics) and quantified by ImageJ 1.53f51 software. Primers used are specified in **Supplementary Table 6**.

In-vitro kinase assay

HCT116 cells were plated onto 150 cm^2 plate to reach 70 % confluency at the day of experiment. Next day the cells were co-transfected with Flag-tagged CDK9 (10 µg), Flag-tagged CDK11 WT/Xpress-tagged Cyclin L1 (10 µg/5 µg), Flag-tagged CDK11 G579S/ Xpress-tagged Cyclin L1 (10 µg/5 µg) and Flag-tagged CDK11 KD/ Xpress-tagged Cyclin L1 (10 µg/5 µg) with PEI transfection reagent. Media were changed 2.5 h after transfection. The cells were harvested 48 h after transfection, washed twice with PBS and lysed in 1 ml of HEPES buffer (20 mM HEPES-KOH (pH = 7.9), 300 mM KCl, 0.2 % NP-40, 15 % glycerol, 1 mM DTT and protease inhibitors, Sigma, P8340) for 20 min. During the lysis, protein extracts were mildly sonicated (10 x 1s, amp 0.30, using 5/64 probe, QSonica Q55A). Clarified extracts (10,000 g for 10 min at 4°C) were subsequently rotated with 15 µl of packed Flag agarose M2 affinity beads (Sigma, A2220) for 1 h at 4°C. The beads were washed three-times with 1 ml of high salt buffer (20 mM HEPES-KOH (pH = 7.9), 500 mM KCl, 0.2 % NP-40, 15 % glycerol, 1 mM DTT) rotating for 5 min at 4°C

during each wash, followed by one detergent free wash (20 mM HEPES-KOH (pH = 7.9), 150 mM KCl, 15 % glycerol, 1 mM DTT). The remaining buffer was carefully removed and 3xFlag-tagged proteins were eluted using 80 µl of Flag elution buffer (20 mM HEPES-KOH (pH=7.9), 150 mM KCl, 1 mM DTT and 0.238 mg/ml 3xFlag peptide, Sigma, F4799). Each kinase reaction contained either solvent or defined concentration of inhibitor (DMSO, OTS964 and pladi B) diluted in 0.6 µl, 400 ng of human full-length GST-CTD or 500 ng of purified GST-tagged SF3B1 (1-463) (as a reaction substrates) diluted in 48 µl of kinase buffer (20 mM HEPES-KOH (pH = 7.9), 5 mM $MgCl_2$, 2 mM DTT, 1 mM ATP), and 12 µl of eluted 3xFlag-tagged kinase. Kinase reactions were incubated at 30°C for 1 h. Reactions were stopped by adding 15 µl of 3× Laemmli buffer and boiled for 3 min. Kinase reactions were run on SDS-PAGE and the following antibodies were used for detection: Flag (Sigma F3165, 1:3000), Phospho-Ser2 (Chromotek 3E10, 1:500), Phospho-Ser5 (Chromotek 3E8, 1:500), GST (Santa Cruz sc-138, 1:200), CDK9 (Santa Cruz sc-484, 1:1000), Cyclin T1 (Santa Cruz sc-10750, 1:2000), CDK11 (rabbit antiserum, 1:3000), SF3B1 P-T313 (Cell Signaling 25009S, 1:2000) and SF3B1 P-T235 (rabbit antiserum, 1:1000).

RNA-seq

HCT116 cells were plated onto 60 cm^2 plates to reach 50 % confluency at the day of experiment. Next day cells were treated with solvent (DMSO) or 30 nM OTS964 for 4 h. Plates were washed twice with ice-cold PBS 4 h after treatment, scraped, pelleted at 200 g for 3 min and treated for 5 min with 500 µl of cytoplasmic lysis buffer (10 mM Tris-Cl (pH = 8), 0.32 M sucrose, 3 mM $CaCl_2$, 2 mM $MgCl_2$, 0.1 mM EDTA, 0.5 % TritonX-100, supplemented with 40 U/ml RNase inhibitor, Roche, 3335402001). Cytoplasmic RNA present in the supernatant was removed by centrifugation (500 g for 3 min). Nuclear pellets were treated once more with 500 µl of cytoplasmic

lysis buffer and supernatant was completely removed after centrifugation (500 g for 3 min). Nuclear RNA was isolated from the remaining nuclear pellet using Tri-Reagent (Sigma, 93289). 600 ng of DNase treated RNA (Sigma, AMPD1) was used for rRNA depletion using RiboCop rRNA Depletion Kit (Lexogen, #144). Sequencing libraries were prepared using the NEBNext Ultra II Directional RNA Library Prep Kit for Illumina (NEB, E7760) according to the manufacturer's protocol and sequenced on Illumina HiSeq 2500 (VBCF, Vienna) 125 bp paired-end, minimum 100 mil reads per condition in 2 biological replicates.

iCLIP-seq

iCLIP was performed as previously described [19,57] with only minor modifications described below. Briefly, HCT116 cells were plated onto 150 cm2 plates to reach 75% confluency at the day of crosslinking by UV-C (254 nm, 200 mJ/cm2). The cells were treated with either DMSO or 50 nM OTS964 or 186 nM pladi B for 1 h. Composition of all buffers was the same as described in [57]. Each cell pellet (50 µl of packed cells) was lysed in 1 ml of lysis buffer and the lysate was homogenized by passing three-times through an insulin syringe (B.BROWN, Omnican U-100, 32G). The lysate was treated with 4 U/ml Turbo DNase (Thermo Fisher Scientific, AM2238), 12 U/ml RNase I (Thermo Fisher Scientific, AM2295) shaking at 1100 rpm and 37°C for 3 min. Clarified extracts (21,000 g for 30 min) were incubated for 2 h with 2 µg of antibody (SF3B1, Abcam ab66774; U2AF65, Santa Cruz sc-53942; AQR, Bethyl A302-547A) pre-bound to 50 µl of protein G Dynabeads. After series of stringent washes, adenylated L3 RNA adapter was ligated to the 3' end of crosslinked RNAs. Crosslinked protein-RNA complexes were resolved by SDS-PAGE (NuPAGE 4-12% Bis-Tris Protein Gel, Thermo Fisher Scientific, NP0322) and transferred to nitrocellulose membrane. The region of the membrane containing radioactively labelled

crosslinked protein–RNA complexes was excised, RNA was isolated and reverse transcribed to cDNA (technical replicates were mixed together after this step). cDNA was size-selected using urea denaturing gel electrophoresis and three fractions running between 70-85 nt (L-low), 85-120 nt (M-medium) and 120-200 nt (H-high) were isolated. Each fraction was independently circularized by single-stranded DNA ligase, annealed to an oligonucleotide complementary to the restriction site and cut between the two adapter regions by BamHI. After final PCR amplification using P3 and P5 Solexa primers all three fractions were pooled together in ratio 1:5:5 (L:M:H). Multiplexed libraries were sequenced as 50 bp single-end reads on Illumina HiSeq 2500 (VBCF, Vienna).

Isolation and analyses of chromatin-associated proteins and RNAs

Chromatin associated RNA was isolated according to the protocol published by [48]. Briefly, cell pellets (approximately 20-30 µl of packed cell pellet) were re-suspended in 20 mM HEPES (pH = 7.5), 10 mM KCl, 250 mM sucrose, 5 mM $MgCl_2$, 1 mM EGTA, 1 mM PMSF, 1 µl/ml RNasin (Thermo Fisher, 100000840), 1x phosphatase inhibitor cocktail (Sigma, P0044) and 1x protease inhibitor cocktail (Sigma, P8340), and lysed by addition of digitonin (Sigma, D141), 200 µg/ml final concentration at 4°C for 10 min. Nuclei were pelleted by centrifugation (650 g, 5 min) following re-suspension in buffer containing 20 mM Tris-HCL (pH = 7.5), 75 mM NaCl, 0.5 mM EGTA, 50 % glycerol, 1 mM PMSF, 1 µl/ml RNasin, 1x protease and 1x phosphatase inhibitors. Chromatin was extracted by the addition of ten volumes of a solution containing 20 mM HEPES (pH = 7.6), 7.5 mM $MgCl_2$, 0.2 mM EGTA, 300 mM NaCl, 1 M urea and 1 % NP-40 at 4°C for 10 min. After centrifugation (650 g, 5 min), chromatin pellet was diluted in 1 ml of Tri-Reagent (Sigma, 93289), carefully homogenized by vigorous pipetting and frozen at -80°C. RNA was

isolated according to the manufacturer's protocol. After DNase treatment (AMPD1, Sigma), 1 µg of RNA was reverse-transcribed using random hexamers (IDT DNA) and Superscript III reverse transcriptase (Thermo Fisher). Resulting cDNA was further diluted with water (40×) and 5 µl of diluted cDNA served as a template for each qPCR reaction using SYBR Green JumpStart TaqReadyMix (Sigma, S4438) with the following parameters: 95°C for 2 min followed by 45 cycles of denaturation at 95°C for 15 s, annealing at 55°C for 30 s and extension at 72°C for 30 s. Primers used are specified in **Supplementary Table 6**. Real-time qPCRs were performed on Aria Mx instrument (Agilent) in triplicate for each biological replicate and error bars represent standard error of the mean of four biological replicates.

For analyses of chromatin-associated proteins, the chromatin pellet was diluted in 200 µl of RIPA buffer (50 mM Tris-Cl (pH = 8), 150 mM NaCl, 5 mM EDTA, 1 % NP-40, 0.5 % sodium deoxycholate, 0.1% SDS, supplemented with protease inhibitors, Sigma, P8340) and 100 µl of 3× SDS sample buffer, kept at room temperature for 30 min with occasional shaking, sonicated 30 times for 1 s (amplitude 0.30) using a 5/64 probe (QSonica Q55A) and boiled for 3 min at 95°C. Protein levels were analyzed by SDS-PAGE with the following antibodies: U1-70K (Santa Cruz sc-390899, 1:1000), SF3B1 (MBL MB-D221-3, 1:2000), SNU114 (Novus NBP2-92930, 1:1000), SNU13 (Novus NBP1-32732, 1:500), SMU1 (Santa Cruz sc-100896, 1:200), MFAP1 (Bethyl A304-647A, 1:2000), SNIP1 (Proteintech 14950-1-AP, 1:1000), AQR (Bethyl A302-547A, 1:2000), CDK11 (rabbit antiserum, 1:3000), RNAPII (Cell Signaling #14958, 1:1000), Phospho-Ser2 (Chromotek 3E10, 1:500), FUS (Santa Cruz sc-47711, 1:10000) and Histone H2A (Abcam ab18255, 1:10000).

RNA immunoprecipitation (RIP)

50 µl of Dynabeads per one immunoprecipitation were washed three times with NET-2 buffer (50 mM Tris-HCl, (pH = 7.4), 150 mM NaCl, 0.05 % NP-40) and incubated with 3 µg of SF3B1 antibody (MBL MB-D221-3) or 10 µl of P-T235-SF3B1 antibody (rabbit antiserum) at 4°C for 3 h. HCT116 cells were seeded onto 150 cm^2 plates to reach 75% confluency at the day of treatment. The cells were treated either with DMSO or 50 nM OTS964 for 2 h. Chromatin pellets were isolated as described above and washed once with MNase reaction buffer (NEB, M0247S). Then the pellets were incubated with MNase at 37°C for 90 s with shaking on a thermomixer (1,400 r.p.m.). The reaction was stopped with 10 µl of 250 mM EGTA. Chromatin extracts (120 µl) were clarified by centrifugation (16,000 g for 10 min) and diluted into 580 µl NET-2 buffer. 70 µl of the lysate was taken aside as input, mixed with 1 ml of Tri-Reagent (Sigma, 93289), homogenized, and frozen at -80°C. Remaining lysate (630 µl) was immunoprecipitated with antibody pre-bound Dynabeads for 1 h. Subsequently, the beads were washed with low-salt buffer (20 mM Tris-HCl, (pH = 8), 150 mM NaCl, 2 mM EDTA, 1 % Triton X-100, 0.1 % SDS), high-salt buffer (20 mM Tris-HCl, (pH = 8), 500 mM NaCl, 2 mM EDTA, 1 % Triton X-100, 0.1 % SDS), LiCl buffer (20 mM Tris-Cl, (pH = 8), 250 mM LiCl, 2 mM EDTA, 1 % NP-40, 1 % sodium deoxycholate) and twice with TE buffer (10 mM Tris-Cl, (pH = 8), 1 mM EDTA). Finally, the beads were mixed with 1 ml of Tri-Reagent (Sigma, 93289), and frozen at -80°C. RNA from the immunoprecipitation and input samples was isolated according to the manufacturer's protocol. After DNase treatment (Sigma, AMPD1), RNA was reverse-transcribed using random hexamers (IDT DNA) and Superscript III reverse transcriptase (Thermo Fisher). Resulting cDNA was further diluted with water (40×) and 5 µl of the diluted cDNA was used for qPCR reaction (95°C for 2 min followed by 45 cycles of denaturation at 95°C for 15 s, annealing at 55°C for 30 s and extension at 72°C for 30 s) using SYBR Green JumpStart TaqReadyMix kit (Sigma, S4438). Primers are specified in

Supplementary Table 6. Real-time qPCR was performed on Aria Mx instrument (Agilent) in triplicate for each biological replicate and error bars represent standard error of the mean of four biological replicates. Percentage of immunoprecipitated snRNA was determined as described [58]. Briefly, DMSO treated input sample was used for preparation of calibration curve. Relative amounts of other input (OTS964, noAb) and all immunoprecipitation (IP) (DMSO, OTS964, noAb) samples were calculated based on the DMSO input calibration curve. Finally, IP/input ratios were calculated and plotted as average of four biological replicates, error bars represent standard errors.

Preparation of HCT116 CDK11 G579S and HCT116 SF3B1 R1074H cell lines

To prepare HCT116 CDK11 G579S and HCT116 SF3B1 R1074H cell lines, we followed reports by [22] and [59], respectively. Briefly, HCT116 WT cells were seeded on 150 cm^2 plate to approximately 30 % confluency. Selection with OTS964 (HY-12467, MedChemExpress) or pladi B (Cay16538-100, Cayman Chemical) started the following day. Resistant cell line was selected in Dulbecco's modified Eagle's medium (DMEM, D6429-500ML, Sigma) containing 5 % FBS (F7524-500ML, Sigma) and 200 nM OTS964 or 4 nM pladi B. The medium was replaced every 4 to 5 days until resistant colonies were formed. Individual colonies were isolated, expanded and checked for the CDK11 G579S or SF3B1 R1074H mutation by PCR (using primers specified in **Supplementary Table 6**) and Sanger sequencing. HCT116 SF3B1 R1074H cell line had a small basal splicing defect on *Riok3* gene (**Extended Fig. 3d**).

Sulforhodamine B cell viability assay

HCT116 WT and resistant HCT116 CDK11 G579S cells were seeded at 5000 cells/well into two 96-well plates and incubated overnight. The first plate (without inhibition) was fixed for 1 h by addition of ice-cold trichloroacetic acid (TCA) (Sigma, T9159) to final concentration 10% to represent 0 h time-point. The second plate was fixed after 72 h of OTS964 treatment (final concentration between 0 and 400 nM). After TCA fixation the plates were washed five times with distilled water and air-dried at room temperature. Fixed cells were stained with 0.4% (w/v) sulforhodamine B (SRB) (Sigma, S1402) in 1% acetic acid at room temperature for 10 min. SRB was quickly washed out by 1% acetic acid to remove unbound dye. Plates were air-dried and SRB was solubilized by addition of 100 µl of unbuffered 10 mM Tris base (pH=10.5) to each well and the plate was left shaking for at least 5 min. Optical density was measured at 515 nm. Measured optical densities were used to calculate fraction of control cell growth as described [60]: fraction of control cell growth = $(\text{meanOD}_{\text{sample}} - \text{meanOD}_{\text{day 0}})/(\text{meanOD}_{\text{neg. control}} - \text{meanOD}_{\text{day 0}})$. Data were fitted to a 4-parameter log-logistic curve (LL.4) with upper bound fixed at 1 using package drc (version 3.0-1) in R statistical software (version 4.0.3)[61].

Cell cycle analysis

HCT116 WT or HCT116 CDK11 G579S cells plated at 50–60 % confluency onto 60 cm^2 plates were grown in the presence of 50, 200 or 400 nM OTS964 or in DMSO for 16 h. Cell cycle profile was measured by flow cytometry based on the DNA content of cells using propidium iodide (PI) (Sigma, P4170) staining as described previously [62]. Briefly, the trypsinized cells were washed twice with PBS, fixed with ice-cold 70 % (v/v) ethanol and stored at −20°C. At the day of measurement, the fixed cells were washed twice with ice-cold PBS and resuspended in Vindal buffer (10 mM Tris–Cl (pH = 8), 1 mM NaCl, and 0.1 % Triton X-100) containing freshly added

PI (50 µg/ml) and RNase A (200 µg/ml; Qiagen, 19101) and incubated at room temperature for 20 min before measurement by BD FACSVerse (BD Bioscience) using flowing software BD FACSuite v1.0.6.5230 (Turku Bioscience Centre). Cell cycle distribution was analyzed by FLOWING version 2.1 software.

4SU-seq

HCT116 cells plated at 50-60 % confluency onto 150 cm^2 dishes were treated with 186 nM pladi B for 45 min, 50 nM OTS964 for 15 min or DMSO for 15 min in 10 ml of DMEM at 37°C. Five ml of the medium were removed and saved. The cells were treated with 500 nM 4SU and incubated at 37°C for another 15 min. For pulse experiment, medium was discarded and the cells were lysed in 3 ml of TriReagent at room temperature for 5 min and then stored at -80°C. For chase experiment, the cells were washed once in PBS, saved medium was returned into dishes, and the cells were incubated at 37°C for another 2 h. Cells were lysed in 3 ml of TriReagent at room temperature for 5 min and then stored at -80°C.

Thawed samples were mixed with 1 ml of chloroform, centrifuged 12000 g/4°C/20 min and aqueous phase was transferred into new tubes followed by addition of 1.5 ml of precipitation buffer (1.2 M NaCl, 0.8 M sodium citrate) and 1.5 ml of isopropanol. After 10 min incubation at room temperature, the samples were centrifuged 12,000 g/4°C/20 min, the pellets were washed with 1 ml of 75 % EtOH, centrifuged 13,000 g/4°C/10 min and diluted in 100 ul of RNase-free water. After 10 min incubation at 65°C, the samples were immediately cooled on ice and stored at -80°C. Biotinylation was performed as described previously [63], [64]. Reaction consisted of 100 µg of RNA, 0.01 mg/ml MTSEA Biotin-XX (Biotium, 90066), 20 % DMF, 10 mM Tris (pH = 7.4), 1 mM EDTA. The samples were incubated at room temperature for 30 min in the dark and RNA was

extracted twice by chloroform extraction in Phase Lock Gel Heavy tubes (Quantabio, 71386). RNA was precipitated for 10 min at room temperature using 1/10th volume of 5 M NaCl and 1 volume of isopropanol, and centrifuged 20,000 g/4°C/20 min. RNA was diluted in 80 ul of RNase-free water, heated at 65°C for 10 min, immediately cooled on ice and 5 ul of wash buffer (100 mM Tris (pH = 7.4), 10 mM EDTA, 1 M NaCl, 0.1 % Tween-20) was added.

Dynabeads MyOne Streptavidin C1 (Thermo Fisher, 65001, 50 ul/sample) were washed twice in 500 ul of RNase-free water, twice with 500 ul of wash buffer and blocked in 440 ul of wash buffer containing 40 ng/ml GlycoBlue (Ambion, AM9516) for 1 h at room temperature in the dark. The beads were washed twice with 500 ul of wash buffer, split into new tubes and biotinylated RNA was added. The samples were incubated for 15 min at room temperature in the dark, washed 4x with 0.9 ml of wash buffer and eluted for 15 min at room temperature with 100 ul of elution buffer (100 mM Tris (pH=7.4), 1 mM EDTA, 100 mM NaCl, 0.01 % Tween 20). Elution was repeated once and eluates were pooled. The eluates were cleaned using RNeasy MinElute Kit (Qiagen, 74204) with final elution into 25 ul of RNase-free water.

The samples (550 ng of RNA) were treated with DNase I (Sigma, AMPD1) according to the manufacturer's protocol. KAPA Pure Beads (Roche, 07983271001, 2.2× sample volume) were used for cleanup, incubated for 15 min at room temperature, and washed twice in 80% ethanol. The samples were eluted into 15 ul of RNase-free water.

Libraries were prepared using 450 ng of RNA and Lexogen SiRV – Set 3 spike-ins (180 pg). Ribosomal RNA depletion was done using RiboCop rRNA Depletion Kit version 1.3 (Lexogen, 037.24) following the manufacturer's instructions. In final step, RNA was eluted into 6.5 ul of RNase-free water and 5 ul of this eluate were used for library preparation.

971 Libraries were prepared following instructions in NEB Next UltraII Directional RNA Library Kit
972 for Illumina using KAPA Pure Beads. The libraries were sequenced as single-read 50 bp reads on
973 Illumina HiSeq 2500 (VBCF, Vienna).
974
975 **Identification of CDK11-associated proteins by immunoprecipitation coupled to LC-MS/MS**
976 HEK293 cells with stably integrated control 3xFlag-tagged empty vector (F-EV) and 3xFlag-
977 tagged CDK11 (F-CDK11)[19] were grown to reach 80 % confluency. Leaky (uninduced) expression
978 of F-CDK11 was comparable to endogenous CDK11, thus the protein expression was not induced
979 by doxycycline. Twenty-five 150 cm^2 plates were used for each immunoprecipitation condition,
980 i.e. for F-EV, F-CDK11 and F-CDK11+RNase A. Equal expression levels of F-CDK11 and
981 endogenous CDK11 were confirmed by western blotting with CDK11 antibody (rabbit antiserum,
982 1:3000).
983 The cells from twenty-five 150 cm^2 plates were harvested and spun at 1,000 g for 5 min. The pellet
984 was washed with 20 ml of room temperature PBS and lysed gently with 20 ml of ice-cold
985 cytoplasmic lysis buffer (0.05 % NP-40, 10 mM HEPES-KOH (pH = 7.9), 1.5 mM $MgCl_2$, 10 mM
986 KCl, Complete EDTA free protease inhibitor (5056489001, Roche)). The cells were incubated on
987 ice for 15 min, the lysate spun at 1,000 g at 4°C for 10 min, the supernatant was then removed and
988 pelleted nuclei kept on ice. The pellet was lysed in 12.5 ml of DNase buffer (20 mM HEPES-KOH
989 (pH = 7.9), 10 % glycerol, 1.5 mM $MgCl_2$, 1 mM DTT, Complete EDTA free protease inhibitor
990 and 6.25 µl of EDTA free RNase inhibitor (3335402001, Roche)). The RNase inhibitor was
991 omitted from buffers used for sample treated with RNase A. Lysed nuclei were poured to Dounce
992 homogenizer and homogenized on ice with 10 strokes of tight pestle B. Homogenized nuclei were
993 lightly sonicated on ice (Qsonica 55, amplitude 30, five bursts for 5 seconds) and treated with

DNase Turbo (AM2238, Ambion, Life technologies, 25 U (12.5 µl per 1 ml of the lysate)). One sample was also treated with RNase A (19101, Qiagen) to the final concentration of 200 µg/ml. All samples were incubated at room temperature for 30 min. The lysates were adjusted to the final concentration of NP-40 0.2 % and KCl 150 mM, mixed gently and put on ice for 5 min and then cleared with 10,000 g at 4°C for 10 min. The supernatant was precleared with 60 µl of mouse IgG agarose (A0919, Sigma) at 4°C for 30 min on rotator. 100 µl of M2-Flag agarose beads (A2220, Sigma) were prewashed three times with 1 ml of lysis buffer (20 mM HEPES-KOH (pH = 7.9), 150 mM KCl, 0.2% NP-40, 15 % glycerol, 1 mM DTT, Complete EDTA free protease inhibitor) and incubated at 4°C on rotator for 1 h and then spun at 1,000 g for 5 min. The supernatant was removed and the beads with bound proteins were washed twice with 1 ml of lysis buffer containing 150 mM KCl and twice with 1 ml of lysis buffer containing 200 mM KCl. The beads were spun at 1,000 g for 20 sec in between the washes. Finally, the beads were washed twice with 1 ml of detergent-free buffer (20 mM HEPES (pH = 7.9), 150 mM KCl, 1 mM DTT, 15 % glycerol). The buffer was completely removed and Flag-associated proteins were eluted by washing the beads twice with 75 µl of Flag elution solution containing 3 µl of Flag peptide from 5 mg/ml stock solution (F4799, Sigma) and 72 µl of Flag elution buffer (20 mM HEPES (pH = 7.9), 150 mM KCl, 1 mM DTT). Each elution step was done for 10 min at room temperature with continuous gentle shaking. 150 µl of pooled Flag eluates were mixed with 50 µl of 4×SDS sample buffer, boiled at 95°C for 3 min and loaded on 10 % SDS-PAGE gel. The proteins resolved on the gel were stained using ProteinSilver Plus Silver Stain Kit (PROTSIL2-1KT, Sigma) according to the manufacturer´s instructions.

Selected 1D gel bands were excised manually and after destaining and washing procedures each band was subjected to protein reduction (10 mM DTT in 25 mM $NaHCO_3$, 45 min, 56°C, 750 rpm)

and alkylation (55 mM IAA in 25 mM $NaHCO_3$; 30 min, room temparature, 750 rpm) step. After further washing by ACN:25 mM NaHCO3 (1:1) and pure ACN, the gel pieces were incubated with 125 ng trypsin (sequencing grade; Promega) in 50 mM $NaHCO_3$. The digestion was performed for 2 h at 40°C on a Thermomixer (750 rpm; Eppendorf). Tryptic peptides were extracted into LC-MS vials by 2.5% formic acid (FA) in 50% ACN with addition of polyethylene glycol (20,000; final concentration 0.001 %) and concentrated in a SpeedVac concentrator (Thermo Fisher Scientific).

LC-MS/MS analyses of peptide mixtures coming from in-gel digestions were done using Ultimate 3000 RSLCnano system (Thermo Fisher Scientific) on-line connected to Impact II Ultra-High Resolution Qq-Time-Of-Flight mass spectrometer (Bruker, Bremen, Germany). Prior to LC separation, tryptic digests were online concentrated and desalted using trapping column (100 µm × 30 mm) filled with 3.5-µm X-Bridge BEH 130 C18 sorbent (Waters, Milford, MA, USA). After washing of trapping column with 0.1 % FA, the peptides were eluted (flow 300 nl/min) from the trapping column onto an Acclaim Pepmap100 C18 column (2 µm particles, 75 µm × 500 mm; Thermo Fisher Scientific, Waltham, MA, USA) by the gradient program using 0.1 % FA in water and 0.1 % FA in 80% acetonitrile. Equilibration of the trapping column and the analytical column was done before sample injection into sample loop. The analytical column outlet was directly connected to the CaptiveSpray nanoBooster ion source (Bruker). NanoBooster was filled with acetonitrile and nanoBooster pressure was set to 0.2 Bar.

MS data were acquired in a data-dependent strategy with 3 s long cycle time. Mass range was set to 150-2200 m/z and precursors were selected from 300-2000 m/z. Active exclusion was enabled for 2 min after one MS/MS spectra acquisition with Reconsider Precursor option enabled (intensity ratio of 5). Precursor charge state was monitored with exclusion of singly charged precursors.

Acquisition speed of MS and MS/MS scans was 2 Hz and 4-16 Hz, respectively. Speed of MS/MS spectra acquisition was based on precursor intensity (low and high absolute thresholds were 10 000 and 100 000 cts, respectively). Standard CID collision energies and isolation widths with respect to precursor charge and m/z were used.

The pre-processing of the mass spectrometric data including recalibration, compounds detection and charge deconvolution was carried out in DataAnalysis software (4.2 SR1; Bruker). Exported MS/MS spectra were analysed in Proteome Discoverer software (Thermo Fisher Scientific; version 1.4) with in-house Mascot (Matrixscience, London, UK; version 2.4) search engine utilisation. Mascot MS/MS ion searches were done against in-house database containing proteins from *Homo sapiens* (UniProtKB database containing canonical and isoform sequences downloaded on 1.10.2014, number of seqeunces 85893). cRAP contaminant database (downloaded from http://www.thegpm.org/crap/) was searched in parallel to exclude contaminant spectra. Mass tolerance for peptides and MS/MS fragments were 15 ppm and 0.05 Da, respectively. Oxidation of methionine, propionamidation (C) and deamidation (N, Q) as optional modifications, and two enzyme miss cleavages were set for all searches. Database search results against human database were postprocessed using Percolator. Peptides with local false discovery rate (PEP-value) < 1%, rank 1 and with at least 6 amino acids were considered. The mass spectrometry proteomics data have been deposited to the ProteomeXchange Consortium[55] and are available via ProteomeXchange dataset PXD035189 (https://doi.org/doi:10.25345/C59P2W974).

ChIP–seq

ChIP was performed with the following antibodies: 1.5 µg of RNAPII (Cell Signaling #14958), 3 µg of Phospho-Ser2 (Active Motif 61083), 3.5 µg of Phospho-Ser5 (Active Motif 61085) and 3.5

µg of Phospho-Ser7 (Active Motif 61087) in 2 technical replicates. Briefly, 20 µl of protein G Dynabeads (Thermo Fisher Scientific, 10009D) per one immunoprecipitation were pre-blocked with 0.2 mg/ml BSA (Thermo Fisher Scientific, AM2616) for 4 h, washed three times with RIPA buffer (50 mM Tris-Cl, (pH = 8), 150 mM NaCl, 5 mM EDTA, 1 % NP-40, 0.5 % sodium deoxycholate, 0.1% SDS, supplemented with protease inhibitors, Sigma, P8340), followed by the incubation with specific antibody at 4°C for at least 4 h. HCT116 cells were plated onto 150 cm^2 plates to reach 75% confluency at the day of the experiment and then treated with 30 nM OTS964 for 4 h. The cells were crosslinked with 1 % formaldehyde for 10 min, and the reaction was quenched with glycine (final concentration 125 mM) for 5 min. The cells were washed twice with ice-cold PBS, scraped and pelleted. Each 20 µl packed cell pellet was lysed in 650 µl of RIPA buffer and sonicated 20 × 7 s (amplitude 0.85) using a 5/64 probe (QSonica Q55A). Clarified extracts (13,000 g for 10 min) were precleared with protein G Dynabeads (Thermo Fisher Scientific, 10009D) by rotation at 4°C for 2–4 h and the 300 µl of precleared extracts were incubated overnight with antibody pre-bound to protein G Dynabeads. We used 300 µl of clarified extract for RNAPII, P-Ser7, P-Ser5 and P-Ser2. The next day, the beads were washed sequentially with low-salt buffer (20 mM Tris-Cl, (pH = 8), 150 mM NaCl, 2 mM EDTA, 1 % Triton X-100, 0.1 % SDS), high-salt buffer (20 mM Tris-Cl, (pH = 8), 500 mM NaCl, 2 mM EDTA, 1 % Triton X-100, 0.1 % SDS), LiCl buffer (20 mM Tris-Cl, (pH = 8), 250 mM LiCl, 2 mM EDTA, 1 % NP-40, 1 % sodium deoxycholate) and twice with TE buffer (10 mM Tris-Cl, (pH = 8), 1 mM EDTA). The bound complexes were eluted with 500 µl of elution buffer (1 % SDS and 0.1 M $NaHCO_3$). To reverse formaldehyde crosslinks, immunoprecipitated DNA was incubated at 65°C for at least 4 h and was subsequently treated with proteinase K at 42°C for 2 h (10 µg per ml, Sigma P5568) with 2 µl of GlycoBlue added (Thermo Fisher Scientific, AM9516). After phenol:chloroform

extraction (Sigma, P3803), immunoprecipitated DNA was dissolved in 17 µl of water and technical replicates were pooled to get at least 2.5 ng of immunoprecipitated DNA before library preparation (measured by Qubit). ChIP–seq libraries were generated using the KAPA Biosystems Hyper Prep Kit (KK8502) and NEBNext Multiplex Oligos for Illumina (Index Primers Set 1 and Set 2 (NEB E7335S, E7500S)). The libraries were sequenced (50 bp single-end reads) using an Illumina HiSeq 2500 (VBCF Vienna). The experiment was done in two biological replicates.

TOPK protein expression and purification

TOPK full-length protein was expressed and purified from *E. coli* overexpression by standard methods: The constructs were transformed into BL21(DE3) cells that contained the pRARE2 plasmid that expressed rare tRNAs. The resulting colonies were used to inoculate 50 mL of LB media containing 50 µg/mL kanamycin and 34 µg/mL chloramphenicol which was left shaking at 37 °C overnight. This culture was used to inoculate 1 L volumes of LB media containing 35 µg/mL kanamycin at a ratio of 10 mL culture to 1 L fresh media. The cultures were grown at 37 °C with shaking until an OD600 of 0.5 was reached. The temperature was reduced to 20 °C, and when the OD600 reached 0.7 isopropyl β-D-1-thiogalactopyranoside (IPTG) was added to a final concentration of 0.5 mM and the cultures were left overnight. Cells were harvested by centrifugation and re-suspended in Binding Buffer (50 mM Hepes pH 7.5, 500 mM NaCl, 20 mM imidazole, 5% glycerol, 0.5 mM tris(2-carboxyethyl)phosphine (TCEP)).

The re-suspended cells were lysed by sonication, DNase I (Roche, Basel, CH) and cOmplete EDTA-free protease inhibitor (Roche, Basel, CH) were added, and the insoluble debris was removed by centrifugation. The supernatant was passed through a column of 5 mL Ni-Sepharose resin (GE Healthcare). The resin was washed with Binding Buffer containing increasing amounts

of imidazole before elution with Binding Buffer containing 250 mM imidazole. When the expression tag was removed, TEV protease was added to the eluate, which was dialyzed into 20 mM Hepes pH 7.5, 500 mM NaCl, 5 % glycerol, 0.5 mM TCEP (GF Buffer) overnight at 4 °C, and the protein complex was further purified by passing through a gravity column of 3 mL Ni-Sepharose. The flow-through was collected and the column was washed with GF Buffer containing 30, 60, 90, 120 and 250 mM imidazole. Protein was further purified by size exclusion chromatography: the protein sample was concentrated to 5 mL and injected on a HiLoad® 26/600 Superdex® 75 pg (GE Healthcare) pre-equilibrated into GF Buffer. Fractions containing the desired protein were pooled and concentrated by ultrafiltration. Protein identity was confirmed by electrospray ionization mass spectrometry (ESI-MS).

Differential Scanning Flourimetry (DSF)

DSF measurements were performed as described previously[65]. In brief: A 2 µM solution of TOPK was tested with a compound concentration of 20 µM adding 5x Sypro Orange (Thermo, #S6650) to the solution. Measurements of the fluorescence curve was performed using a QuantStudio 5 (Thermo) in a temperature range from 25°C to 85°C. GraphPad Prism 9 was used for determination of the melting point (Boltzmann-Fit) which was then compared to the wild-type melting point of the individual protein as determined in an experiment without compound but DMSO addition (vehicle control).

Isothermal Titration Calorimetry (ITC)

The ITC measurement was performed as described[66] using a NanoITC (TA instruments) at 25 °C in buffer (50 mM HEPES pH 7.5, 500 mM NaCl, 0.5 mM TCEP and 5% Glycerol). TOPK (100

μM) was injected into the cell that contained OTS964 (10 μM). The integrated heat of the titration was calculated and fitted to a single, independent binding model using the software provided by the manufacturer. The data was graphed using GraphPad Prism 9.

Kinome-wide profiling and radiometric assays

The kinome-wide profiling at 1 μM concentration of the compound (**Supplementary Table 1, Fig. 1a)** was performed by Eurofins (using Km concentrations of ATP)**.** The IC50 values were determined using radiometric assays in Eurofins, using Km concentrations of ATP (**Supplementary Table 2, Supplementary Data File 1)** and Reaction Biology, using 10 □M concentration of ATP (**Extended Fig. 1a**).

Generation of phospho-specific SF3B1 antibodies

The custom-made antibodies were prepared by Moravian-Biotechnology Ltd. (Brno, Czech Republic). Briefly, the antibodies targeting P-Thr211, P-Thr235 and P-Thr328 SF3B1 were raised against the peptides [10] injected into rabbits. Rabbit serum was affinity purified through peptide affinity columns using SulfoLink kit (Pierce). 15 ml of the serum was incubated with non-phosphopeptide column to remove non-phospho-specific IgG and the procedure was repeated one more time. The flow-through was collected and purified via phospho-affinity column to pull down phospho-specific IgG. The purified IgG was eluted with 100 mM glycine (pH = 2.5) and stabilized with 1 M Tris buffer (pH = 8). All the phospho-specific SF3B1 antibodies were validated using phosphatase and dot blot/western blotting probed either with the phospho-specific or total (MBL MB-D221-3, 1:2000) SF3B1 antibodies. Additionally, the antibodies were characterized in

immunoprecipitation experiments and the P-Thr235 and P-Thr211 were found to be suitable for the immunoprecipitation.

RNA-seq and ChIP-seq analyses

Quality check of RNA-seq reads was performed using fastQC (available online at: http://www.bioinformatics.babraham.ac.uk/projects/fastqc). RNA-seq reads were mapped against the human genome (hg38) and human rRNA sequences using ContextMap version 2.7.9 [67] using BWA [68] as short read aligner and default parameters. Number of read counts per gene and exon were determined from the mapped RNA-seq reads in a strand-specific manner using featureCounts [69] and gene annotations from from Ensembl version 100.

Differential gene expression analysis was performed using DESeq2 [70]. P-values were adjusted for multiple testing using the method by Benjamini and Hochberg [71] and genes with an adjusted p-value ≤ 0.01 were considered significantly differentially expressed. Analysis workflows were implemented and run using the Watchdog workflow management system [72].

ChIP-seq reads were aligned to the human genome (hg38) using BWA [68]. Reads with an alignment score <20 were discarded.

Read coverage per genome position was calculated using the bedtools genomecov tool [73]. RNA-seq and ChIP-seq read coverage was visualized using the Integrative Genomics Viewer (IGV) [74]. Creation of other figures and statistical analysis of RNA-seq and ChIP-seq data were performed in R (R Core Team (2016). R: A language and environment for statistical computing. R Foundation for Statistical Computing, Vienna, Austria. URL https://www.R-project.org/.)

Metagene analysis

The metagene analysis of read coverage distribution in ChIP-seq data was restricted to high confidence transcripts of protein-coding genes annotated in Ensembl version 100. Transcripts shorter than 3,180 bp were excluded. Furthermore, only the genes with a distance of ≥5000nt from the next gene were included. Among these, the 7500 genes with the highest coverage in the RNAPII DMSO ChIP-seq data were selected for the metagene analysis. For each gene, we selected the transcript with the most read counts in the RNAPII DMSO ChIP-seq samples (normalized to library size) in the ±3 kb regions around the transcription start site (TSS) and transcription termination site (TTS). For each gene, the regions −3 kb to +1.5 kb of the TSS and −1.5 kb to +3 kb of the TTS were divided into 50 bp bins (180 bins in total) and the remainder of the gene body (+1.5 kb of TSS to −1.5 kb of TTS) into 180 bins of variable length in order to compare genes with different lengths. For each bin, the average coverage per genome position was then calculated and normalized to the total sum of average coverages per bin such that the sum of all bins was 1. Finally, metagene plots were created by averaging results for corresponding bins across all genes considered. To determine statistical significance of differences between inhibitor and control, paired Wilcoxon signed rank tests were performed for each bin comparing normalized coverage values for each gene for this bin with and without the inhibitor. *P*-values were adjusted for multiple testing with the Bonferroni method across all bins within each subfigure and are color-coded in the bottom track of each subfigure: red = adj. *P*-value ≤ 10−15; orange = adj. *P*-value ≤ 10−10; yellow: adj. *P*-value ≤ 10−3.

Analyses of promoter-proximal pausing

Pausing indices (PI) were calculated from the ChIP-seq data for the transcripts included in the metagene analysis by calculating reads counts per kilo base of length (RPK) in the promoter region

(-250 nt of the TSS to +250 nt of the TSS) and dividing this by the gene body RPK (= RPK for the region from +250 nt of the TSS to +2000 nt from the TSS).

Major isoform selection and splicing ratio analysis

Major expressed transcript isoforms were selected as described previously [75]. RNA-seq was analyzed using a Nextflow pipeline [76] from the NF-Core consortia (https://github.com/nf-core/rnaseq v3.0). In order to select the major isoform, reads were aligned with Salmon (0.14.1) [77] to curated RefSeq annotated isoforms (UCSC RefSeq GRCh38, downloaded in May 2021). For each gene the major isoform was selected as the maximum mean of Transcripts Per Million (TPM) across all samples, considering gene isoforms with more than 70%. Additionally, major isoforms associated with overlapping genes as well as isoforms located on chromosomes X, Y and M were discarded from further analysis. The final major isoform annotation includes 6,622 isoforms containing 60,809 exons and 54,587 introns.

To calculate splicing ratio an exon-based splice junction analysis was performed [75]. Exons from major isoforms containing a first exon > 100 bp were included, and major isoforms with a single annotated exon were excluded. A window of ± 4 bp around the splice junction (2 bp in the exon and 2 bp in the intron) was defined to investigate spliced and unspliced reads by means of the findOverlaps function from the GenomicRanges R package version 1.42 [78]. Unspliced reads were defined as the ones overlapping at least 3 bp of the defined window and total reads (spliced and unspliced) the ones spanning at least 2 bp of the defined window. Afterward, the number of spliced reads was calculated by the difference between total and unspliced reads. The splicing ratio was calculated by dividing the number of spliced reads by the total amount of spliced and unspliced reads [75].

iCLIP data analysis

U2AF65, SF3B1 and AQR iCLIP sequencing reads were processed on the iMaps server using the iCount software (https://github.com/tomazc/iCount). Briefly, experimental barcodes were removed and sequencing reads aligned with STAR [79] to hg38 human reference genome (build GRCh38 primary assembly GENCODE version 27), allowing two mismatches and ten secondary alignments. Unique Molecular Identifiers (UMIs), were used to distinguish and remove PCR duplicates. To determine protein-RNA contact sites, the uniquely mapped sequencing read preceding nucleotide was assigned as the crosslink site event.

Assignment of crosslink sites to coding transcripts, non-coding or biotype features, was done by the following segmentation hierarchy rules (https://github.com/tomazc/iCount/blob/master/iCount/genomes/segment.py). Then, replicate correlation was confirmed with Pearson [80] using 10 nt bins and merged accordingly. Summary of cDNA counts within genes and genic regions was generated with iCount summary function after normalising the counts by the length of corresponding regions.

Significant contact sites were identified as iCLIP peaks, using the iCount peak function, based on false discovery rate (FDR) < 0.05 comparing specific sites within a window of three nucleotides with randomised data (100 permutations) and within co-transcribed regions (https://github.com/tomazc/iCount/blob/master/iCount/analysis/peaks.py). The significant crosslink signal was normalised by sequencing deep and million of tags (CPM). Combined genome-wide coverage tracks of U2AF65, SF3B1 and AQR iCLIP were generated using deepTools [80] normalised by sequencing deep and million of tags (CPM) and binned per nucleotide.

Density plots were drawn using normalised coverages around the 3'SS [75] using single nucleotide bins.

Data availability

All next-generation-sequencing source and processed data are available at NCBI GEO (accession number GSE185813). Mass spectrometry proteomics data are available via ProteomeXchange dataset PXD035189 (https://doi.org/doi:10.25345/C59P2W974).

Statistics and reproducibility

The results are reported as means ± standard error of the mean (SEM) unless stated otherwise. The following figure panels show representative data from two biologically independent experiments that showed similar results: Fig. 1c, 3a, b, e, Extended Data Fig. 1e, 2a, b, 4a, 6a, b, c, 7b, e, g, h, 8a, b, c, d, e, f, 9a, b, c. The following figure panels show representative data from three biologically independent experiments that showed similar results: Fig. 1b, d, 3d, f, Extended Data Fig. 4a, 7a, d, 9i. The following figure panel shows representative data from four biologically independent experiments that showed similar results: Fig. 4g. The experiment in the Fig. 3c was performed once and the interactions between endogenous CDK11 and SF3B1 were confirmed by three independent immunoprecipitations of endogenous proteins in Fig. 3d and Extended Data Fig. 7a. The experiment in the Extended Data Fig. 1f was performed once and not repeated because even very high concentrations of OTS964 did not inhibit TYK2.

Additional References Associated with Methods

51. Allen, J.J., *et al.* A semisynthetic epitope for kinase substrates. *Nat Methods* **4**, 511-516 (2007).
52. Stejskal, K., Potesil, D. & Zdrahal, Z. Suppression of peptide sample losses in autosampler vials. *J Proteome Res* **12**, 3057-3062 (2013).
53. Cox, J. & Mann, M. MaxQuant enables high peptide identification rates, individualized p.p.b.-range mass accuracies and proteome-wide protein quantification. *Nature biotechnology* **26**, 1367-1372 (2008).
54. Cox, J., *et al.* Andromeda: a peptide search engine integrated into the MaxQuant environment. *J Proteome Res* **10**, 1794-1805 (2011).
55. Perez-Riverol, Y., *et al.* The PRIDE database resources in 2022: a hub for mass spectrometry-based proteomics evidences. *Nucleic acids research* **50**, D543-D552 (2022).
56. Kramer, A., *et al.* Optimization of pyrazolo[1,5-a]pyrimidines lead to the identification of a highly selective casein kinase 2 inhibitor. *Eur J Med Chem* **208**, 112770 (2020).
57. Huppertz, I., *et al.* iCLIP: protein-RNA interactions at nucleotide resolution. *Methods* **65**, 274-287 (2014).
58. Mukherjee, P., Raghava Kurup, R. & Hundley, H.A. RNA immunoprecipitation to identify in vivo targets of RNA editing and modifying enzymes. *Methods Enzymol* **658**, 137-160 (2021).
59. Teng, T., *et al.* Splicing modulators act at the branch point adenosine binding pocket defined by the PHF5A-SF3b complex. *Nature communications* **8**, 15522 (2017).
60. Vichai, V. & Kirtikara, K. Sulforhodamine B colorimetric assay for cytotoxicity screening. *Nature protocols* **1**, 1112-1116 (2006).
61. Ritz, C., Baty, F., Streibig, J.C. & Gerhard, D. Dose-Response Analysis Using R. *PloS one* **10**, e0146021 (2015).
62. Chirackal Manavalan, A.P., *et al.* CDK12 controls G1/S progression by regulating RNAPII processivity at core DNA replication genes. *EMBO reports* **20**, e47592 (2019).
63. Radle, B., *et al.* Metabolic labeling of newly transcribed RNA for high resolution gene expression profiling of RNA synthesis, processing and decay in cell culture. *J Vis Exp* (2013).
64. Duffy, E.E. & Simon, M.D. Enriching s(4) U-RNA Using Methane Thiosulfonate (MTS) Chemistry. *Curr Protoc Chem Biol* **8**, 234-250 (2016).
65. Fedorov, O., Niesen, F.H. & Knapp, S. Kinase inhibitor selectivity profiling using differential scanning fluorimetry. *Methods Mol Biol* **795**, 109-118 (2012).
66. Asquith, C.R.M., *et al.* SGC-GAK-1: A Chemical Probe for Cyclin G Associated Kinase (GAK). *J Med Chem* **62**, 2830-2836 (2019).
67. Bonfert, T., Kirner, E., Csaba, G., Zimmer, R. & Friedel, C.C. ContextMap 2: fast and accurate context-based RNA-seq mapping. *BMC Bioinformatics* **16**, 122 (2015).
68. Li, H. & Durbin, R. Fast and accurate short read alignment with Burrows-Wheeler transform. *Bioinformatics* **25**, 1754-1760 (2009).
69. Liao, Y., Smyth, G.K. & Shi, W. featureCounts: an efficient general purpose program for assigning sequence reads to genomic features. *Bioinformatics* **30**, 923-930 (2014).
70. Love, M.I., Huber, W. & Anders, S. Moderated estimation of fold change and dispersion for RNA-seq data with DESeq2. *Genome biology* **15**, 550 (2014).
71. Benjamini, Y. & Hochberg, Y. Controlling the False Discovery Rate - a Practical and Powerful Approach to Multiple Testing. *J R Stat Soc B* **57**, 289-300 (1995).

72. Kluge, M. & Friedel, C.C. Watchdog - a workflow management system for the distributed analysis of large-scale experimental data. *BMC Bioinformatics* **19**, 97 (2018).
73. Quinlan, A.R. & Hall, I.M. BEDTools: a flexible suite of utilities for comparing genomic features. *Bioinformatics* **26**, 841-842 (2010).
74. Robinson, J.T.*, et al.* Integrative genomics viewer. *Nature biotechnology* **29**, 24-26 (2011).
75. Caizzi, L.*, et al.* Efficient RNA polymerase II pause release requires U2 snRNP function. *Molecular cell* (2021).
76. Di Tommaso, P.*, et al.* Nextflow enables reproducible computational workflows. *Nature biotechnology* **35**, 316-319 (2017).
77. Patro, R., Duggal, G., Love, M.I., Irizarry, R.A. & Kingsford, C. Salmon provides fast and bias-aware quantification of transcript expression. *Nature Methods* **14**, 417-+ (2017).
78. Lawrence, M.*, et al.* Software for Computing and Annotating Genomic Ranges. *Plos Comput Biol* **9**(2013).
79. Dobin, A.*, et al.* STAR: ultrafast universal RNA-seq aligner. *Bioinformatics* **29**, 15-21 (2013).
80. Ramirez, F., Dundar, F., Diehl, S., Gruning, B.A. & Manke, T. deepTools: a flexible platform for exploring deep-sequencing data. *Nucleic acids research* **42**, W187-191 (2014).

Acknowledgements

We thank all members of the Blazek laboratory for discussions throughout the project and helpful comments on the manuscript, Martina Hallegger for protocols and advice regarding in vitro splicing assays, Marek Šebesta for providing GST-CTD, Tomáš Bárta for providing CDK2 antibody, Kateřina Hanáková for assistance with proteomic experiments and Life Science Editors for editing services.

The work was supported by grants from: Czech Science Foundation (21-19266S), the CEITEC (Project CEITEC-Central-European Institute of Technology (CZ.1.05/1.1.00/02.0068), GAMU MUNI/G/1129/2021 to D.B., Deutsche Forschungsgemeinschaft (DFG) (grants FR2938/9-1 and FR2938/10-1) to C.C.F., European Structural and Investment Funds, Operational Programme Research, Development and Education – „Preclinical Progression of New Organic Compounds with Targeted Biological Activity" (Preclinprogress) - CZ.02.1.01/0.0/0.0/16_025/0007381,

project no. LQ1605 from the National Program of Sustainability II (MEYS CR), the project CZ-OPENSCREEN: National Infrastructure for Chemical Biology (LM2018130), Bader Philanthropies and GAMU MUNI/G/1129/2021 to K.P.. CIISB, Instruct-CZ Centre of Instruct-ERIC EU consortium, funded by MEYS CR infrastructure project LM2018127, is gratefully acknowledged for the financial support of the measurements at the CEITEC Proteomics Core Facility. Computational resources were supplied by the project "e-Infrastruktura CZ" (e-INFRA CZ ID:90140) supported by the Ministry of Education, Youth and Sports of the Czech Republic. S.K. and B-T.B are grateful for support by the SGC, a registered charity (no. 1097737) that receives funds from; AbbVie, Bayer AG, Boehringer Ingelheim, the Canada Foundation for Innovation, Eshelman Institute for Innovation, Genentech, Genome Canada through Ontario Genomics Institute [OGI-196], EU/EFPIA/OICR/McGill/KTH/Diamond, Innovative Medicines Initiative 2 Joint Undertaking [EUbOPEN grant 875510], Janssen, Merck KGaA, Merck & Co, Pfizer, Takeda and Wellcome. S.K. is also grateful for support by the German translational cancer network (DKTK) and the Frankfurt Cancer Institute (FCI). S.K. and B-T.B. are grateful for the support by the collaborative research center 1399 “Mechanisms of drug sensitivity and resistance in small cell lung cancer”.

Author Contribution

M.H., P.G., M.R., B.-T.B., Z.S., D.P. and D.B. performed experiments: M.H. performed in vitro splicing, immunoprecipitation assays and *IVKA* with AS CDK11, validated and used P-SF3B1 antibodies for western blotting analyses of SF3B1 phosphorylation in cells and purified SF3B1 for MS/MS analyses of phosphosites; P.G. performed *IVKA* with the CTD substrate, western blotting

analyses of CTD phosphorylation upon OTS964 treatment, iCLIP, RNA-seq, RIP and RT-(q)PCR experiments and isolated and analyzed chromatin-associated spliceosome components; M.R. performed 4SU-seq, ChIP-seq and western blotting analyses of the CTD phosphorylation upon pladi B treatment; B.-T.B. performed DSF, ITC and NanoBRET assays; Z.S. performed GST pulldown, viability and cell cycle assays, *IVKA* with the SF3B1 substrate and generated drug-resistant cell lines; D.B performed purification of CDK11-associated proteins; D.P. performed and analyzed MS/MS experiments. I.R.dL.M., M.K, E.W. and C.C.F. performed bioinformatics analyses: I.R.dL.M. analyzed iCLIP and splicing ratio from RNA-seq; M.K. analyzed ChIP-seq and RNA-seq; E.W. analyzed promoter-proximal pausing and C.C.F analyzed 4SU-seq. K.P. analyzed kinome-wide profiling and radiometric assays. All authors provided critical feedback, discussed the design of experiments and analyzed data, D.B. wrote the initial draft of the manuscript and all authors edited and approved the manuscript, J.U., S.K., Z.Z, K.P., C.C.F and D.B. supervised research and acquired funding.

Competing Interests

B.-T. B. is a co-founder and the CEO of CELLinib GmbH (Frankfurt am Main, Germany); D.B. has received a consulting fee from Proxygen, GmbH. The other authors declare that the research was conducted in the absence of any commercial or financial relationships that could be construed as a potential conflict of interest.

Additional information

Supplementary information

Correspondence and requests for materials should be addressed to Dalibor Blazek

Peer review information

Extended Data Figure Legends

Extended Fig. 1 Characterization of potential off-targets of OTS964

a, b, Graphs show percentage of CDK9/CyclinT1 **(a)** and TOPK **(b)** kinase activities in the presence of increasing concentrations of OTS964 in *IVKAs.* Resulting IC_{50} from n=2 replicates are shown in the graphs.

c, Isothermal Titration Calorimetry (ITC) of TOPK and OTS964.

d, Differential Scanning Fluorimetry (DSF) curve of TOPK and OTS964, staurosporine, DMSO and blank.

e, f, Graphs show percentage of normalized NanoBRET ratio for CDK9/Cyclin T2 upon OTS964 or control dinaciclib treatment (n=2 biologically independent replicates, a representative replicate is shown) **(e)** and for TYK2 upon OTS964 or control AT9283 treatment (n=1 biological replicate) **(f)**.

Extended Fig. 2 OTS964 decreases bulk phosphorylation of all the CTD residues in a CDK11-dependent manner in cells

a, Immunoblot of proteins after treatment of HCT116 cells with indicated concentrations of OTS964 for indicated times.

b, Immunoblot of proteins after treatment of WT or CDK11 G579S HCT116 cells with 50 nM OTS964 or 200 nM flavopiridol for 4 h.

c, d, Graphs show relative levels of mRNA of 14 histone genes in WT or CDK11 G579S HCT116 cells either treated with DMSO or with 50 nM OTS964 **(c)** or 200 nM flavopiridol **(d)** for 4 h. mRNA levels were normalized to *Ppia* mRNA expression and expression in DMSO was set as 1. n=4 biologically independent experiments, error bars=SEM.

e, Sulforhodamine B growth assays in WT and CDK11 G579S HCT116 cells treated with increasing concentrations of OTS964. n=3 replicates of biologically independent experiments.

f, Percentage of HCT116 WT and CDK11 G579S cells in individual cell cycle phases based on flowcytometry profiles of a representative replicate treated with the indicated concentrations of OTS964 for 16 h. n=3 replicates of biologically independent experiments.

Extended Fig. 3 OTS964 and pladi B globally disrupt splicing in a similar way

a, IGV genome browser view of *Brd2* and *Ddx47* genes from RNA-seq treated with 30 nM OTS964 or DMSO (control) for 4 h.

b, Box plots showing ratio of spliced reads over total unspliced and spliced reads in RNA-seq after treatment with DMSO (control) or 30 nM OTS964 for 4 h. First, middle and last introns in selected 6222 isoforms were considered. Boxes represent the range between the first and third quartiles for each condition. Black horizontal lines in boxes show the median. The ends of the whiskers extend the box by 1.5 times the inter-quartile range. n=2 biologically independent experiments.

c, Graph shows change in expression of transcripts of five genes in WT or CDK11 G579S HCT116 cells either treated with DMSO or 200 nM flavopiridol for 4 h. mRNA levels were normalized to *Ppia* mRNA expression and expression in DMSO was set as 1. n=4 biologically independent experiments, error bars=SEM. E-E=primers spanning exon-exon junctions; E-In=primers spanning exon-intron junctions.

d, Box plots showing the ratio of intronic reads over total intronic and exonic reads in 4SU-seq after treatment with DMSO, 50 nM OTS964 and 186 nM pladi B in pulse (upper) and chase (lower) experiment. Two biological replicates (REP1, REP2) are shown. Boxes represent the range between the first and third quartiles for each condition. Black horizontal lines in boxes show the median. The ends of the whiskers extend the box by 1.5 times the inter-quartile range.

e, IGV genome browser view of *Dusp4* and *Fosl1* genes from pulse and chase 4SU-seq experiments.

f, Scatterplots comparing intron ratios in individual genes between DMSO (control) and either OTS964 (left) or pladi B (right) treated HCT116 cells in 4SU-seq pulse experiment.

g, Scatterplots comparing intron ratios in individual genes between OTS964 and pladi B treated HCT116 cells in 4SU-seq pulse (left) and chase (right) experiments.

h, Boxplots showing distribution of $\log_2$ fold changes of intron ratios for individual genes in OTS964 over DMSO and pladi B over DMSO in 4SU-seq chase experiment. n=2 biologically independent experiments. Boxes represent the range between the first and third quartiles for each condition. Black horizontal lines in boxes show the median. The ends of the whiskers (vertical lines) extend the box by 1.5 times the inter-quartile range. Data points outside this range (outliers) are shown as small circles. The y-axis was limited to the range between -2 and 4.

Extended Fig. 4 CDK11 inhibition alters total and modified RNAPII occupancies on genes

a, Immunoblot of proteins after treatment of HCT116 cells with indicated concentrations of pladi B for indicated times.

b, Metagene analyses of RNAPII ChIP-seq occupancies of the 7500 protein-coding genes with highest RNAPII occupancy in DMSO treated control. Only genes separated by ≥5000 nt from other genes are included. Dotted lines indicate transcription start site (TSS), 1500 nucleotides

downstream of TSS, 1500 nucleotides upstream of transcription termination site (TTS) and TTS. The color track at the bottom indicates the significance of paired two-sided Wilcoxon tests comparing DMSO treated control cells and cells treated with 30 nM OTS964 for 4 h. Color code: red = adjusted *P*-value $\leq 10^{-15}$, orange = adjusted *P*-value $\leq 10^{-10}$, yellow = adjusted *P*-value $\leq 10^{-3}$.

c, d, Metagene analyses of RNAPII ChIP-seq occupancies over down-, up- and non-regulated genes in RNA-seq **(c)** and over transcripts with indicated lengths **(d)** upon 30 nM OTS964 or control DMSO treatment in HCT116 cells for 4 h.

e, Scatter plot comparing PI between OTS964 and control DMSO treatment. Genes in red have ≥ 2-fold increase in PI, in green have ≥ 2-fold decrease and in blue are within the 2-fold range. This analysis includes only well-expressed genes with an RPKM ≥ 1 either on the promoter or gene body in control DMSO treatment.

f, Pie chart showing proportion of genes with indicated increases or decreases in PI or with no change.

g, Boxplots showing the distribution of gene body RPKM (reads per kilo base per million mapped reads) for control DMSO and OTS964 treatment for genes with either a decrease or increase in PI. n=2 biologically independent experiments. Boxes represent the range between the first and third quartiles for each condition. Black horizontal lines in boxes show the median. The ends of the whiskers (vertical lines) extend the box by 1.5 times the inter-quartile range. Data points outside this range (outliers) are shown as small circles. The y-axis was limited to the range between 0 and 2.

h, i, Metagene analyses of P-Ser5 **(h)** and P-Ser7 **(i)** occupancies over 7500 genes upon 30 nM OTS964 or control DMSO treatment for 4 h in HCT116 cells.

Extended Fig. 5 CDK11 inhibition alters transcription dynamics

a, Metagene analyses of P-Ser2 ChIP-seq occupancies over 7500 genes. See **Extended Fig. 4b** for legend.

b, c, Metagene analyses of P-Ser2 ChIP-seq occupancies over down-, up- and non-regulated genes in RNA-seq **(b)** and over transcripts with indicated lengths **(c)** upon 30 nM OTS964 or control DMSO treatment in HCT116 cells for 4 h.

d, IGV gene tracks for gene *Cdc25a* and *Riok3* showing RNAPII, P-Ser2, P-Ser5 and P-Ser7 ChIP-seq occupancies in control DMSO and OTS964 treated HCT116 cells for 4 h.

Extended Fig. 6 OTS964 blocks spliceosome before the first catalytic step of splicing

a, b, Native gel analyses of spliceosome complex formation on radiolabeled *AdML* pre-mRNA in HeLa nuclear extracts treated with DMSO or indicated concentrations of OTS964 for indicated times. Identities of spliceosome complexes E, A, B and C are depicted on the side. -ATP corresponds to ATP-depleted nuclear extracts.

c, Native gel analyses of spliceosome complexes upon treatment with OTS964 or indicated concentrations of control compounds or under condition of low concentration of $MgCl_2$. See **Extended Fig. 6a, b** for legend.

Extended Fig. 7 CDK11 binds and phosphorylates the threonine-proline-rich N-terminus of SF3B1

a, Immunoblot analyses of immunoprecipitations of endogenous CDK11 in HEK293 cells. Detected proteins are indicated on the right. CK2a is known CDK11 interacting partner (ref.[21]), IgG=antibody control.

b, Immunoblot analyses of in vitro binding assays of GST-tagged SF3B1 (1-463) purified from *E. coli* and Flag-tagged CDK11 purified from HCT116 cells. Antibodies used are shown on the right.

c, Schematic view of SF3B1 protein and its deletion mutants used in **(d)**.

d, Immunoblot analyses of *IVKA* using Flag-tagged AS CDK11 and Flag-tagged SF3B1, SF3B1 (1-463), and SF3B1 (464-1304) substrates. AS CDK11 remains catalytically active, but has mutated a gatekeeper methionine to glycine (M503G) in its catalytic site to allow the usage of thiophosphate ATP analogs (ref.[38]). This can be detected in substrates by western blotting using an anti-thiophosphate ester (TPE) antibody (ref.[52]). The blots were probed with Flag, CDK11, SF3B1 and TPE antibodies as indicated. Inputs represent aliquots of individual proteins added to the *IVKA*.

e, Immunoblot of proteins after treatment of WT or SF3B1 R1074H HCT116 cells with 50 nM OTS964 for 3 minutes.

f, Depiction of SF3B1 peptides found by IP-MS/MS in HCT116 cells with stably integrated Flag-tagged-SF3B1 treated with control DMSO or 50 nM OTS964 for 1 h; shown peptides were found in at least 3 replicates of control- but not OTS964-treated cells. Phosphorylated threonines and serines are shown in red; bold indicates the phosphorylated residues found in B^{act} complex (ref.[10]). n=4 replicates.

g, Immunoblot of proteins after treatment of WT HCT116 cells with 20 nM dinaciclib for indicated times.

h, Denaturing gel analyses of the radiolabeled *AdML* pre-mRNA and spliced products from *in vitro* splicing reactions in HeLa nuclear extracts treated with DMSO or 1 μM dinaciclib for indicated times (left panel). Native gel analyses of spliceosome assembly on radiolabeled *AdML* pre-mRNA in HeLa nuclear extracts treated with DMSO or indicated concentrations of dinaciclib for indicated times (right panel). See **Fig. 3a, b** for further legend.

Extended Fig. 8 OTS964 and pladi B affect splicing via different mechanisms

a, Immunoblot of proteins after treatment of WT or SF3B1 R1074H HCT116 cells with 186 nM pladi B for indicated times.

b, Immunoblot of proteins after treatment of SF3B1 R1074H HCT116 cells with 50 nM OTS964 for indicated times.

c, Immunoblot of proteins after treatment of CDK11 G579S HCT116 cells with 186 nM pladi B for indicated times.

d, e, DNA gel-visualized RT-PCR analyses of splicing of *Riok3* **(d)** and *Ccnl1* **(e)** genes in WT, CDK11 G579S and SF3B1 R1074H HCT116 cells treated with control DMSO, 50 nM OTS964 or 186 nM pladi B for indicated times. Schema of unspliced and spliced products are depicted on the right and their ratio (spliced/unspliced) on bottom of gels. Markers on the left indicate size in nucleotides (nt) and DNA corresponds to genomic DNA control.

f, Immunoblot analyses of HCT116 cell lysates treated with either 50 nM OTS964 for 4 h or untreated control. Pan P-RS = pan-phospho-RS specific antibody. Long and short correspond to long and short exposures of the film, respectively.

Extended Fig. 9 CDK11 inhibition stalls spliceosome assembly prior to formation of B^{act} complex

a, b, c, Autoradiography visualization of RNA-$U2AF^{65}$ **(a)**, -SF3B1 **(b)** and -AQR **(c)** complexes resolved on SDS-PAGE gel upon indicated treatments. Clamps on the side of the panels and asterisks indicate RNA-protein complexes upon low (L) and collapsed RNA-protein band upon high (H) RNase I treatments, respectively. REP1=replicate 1; REP2=replicate 2.

d, Correlation analyses between indicated biological replicates of $U2AF^{65}$, SF3B1 and AQR iCLIP libraries (10 kb bins). Numbers correspond to R^2 (Pearson correlation coefficient) between indicated replicates and correlation strength is indicated by the color code.

e, f, g, Graphs show percentage of significantly bound genomic regions (FDR>0.05) and normalized to region length for U2AF^{65} **(e)**, SF3B1 **(f)** and AQR **(g)** iCLIP upon indicated treatments. REP1=replicate 1; REP2=replicate 2.

h, IGV genome browser view of SF3B1, U2AF^{65} and AQR iCLIP binding upon indicated treatments at *Rpl27a* transcript.

i, Immunoblot analyses of association of indicated splicing factors in nucleoplasmic (soluble) and chromatin (chrom) fractions upon treatment with OTS964 in either HCT116 (WT) or HCT116 CDK11 G579S cells. Presence of the factors in specific spliceosome complexes is indicated on the right. Arrows mark phosphorylated (upper) and non-phosphorylated (lower) forms of RNAPII and SF3B1.

Extended Fig. 10 Phosphorylated SF3B1 mediates interaction with snRNAs in the CDK11-dependent manner/Model

a, b, Graphs represent RIP analyses of total **(a)** and P-Thr235 **(b)** SF3B1 binding to indicated snRNAs in HCT116 cells treated with either control DMSO or 50 nM OTS964 for 2 h. n=4 biologically independent experiments, error bars=SEM, no Ab corresponds to no antibody control immunoprecipitation. Lower panels represent zoom-in of upper panels.

c, Graph presents ratios of P-Thr235-SF3B1 and total SF3B1 RIP-qPCR signals on indicated snRNAs. n=4 biologically independent experiments, error bars=SEM. Lower panel represents zoom-in of the upper panel.

d, Working model: CDK11 and its inhibition by OTS964 in pre-mRNA splicing. In untreated cells (no inhibitor), U1 and U2 snRNPs (U1 and U2) are bound on 5' and 3'SS, respectively and unphosphorylated SF3B1 is bound on BP adenosine (A) via HEAT-repeat domain in its "closed" formation, rendering the A complex. Unwinding of U1 and recruitment of U4/U6.U5 tri-snRNPs

(U4/U6, U5) together with B-specific proteins (B-spec.) marks formation of the B complex. During its conversion into B^{act} complex, CDK11 phosphorylates (P) the N-terminus of SF3B1, U4 and B-specific proteins are evicted, and RES and IBC complexes and other B^{act}-specific proteins (B^{act} spec.) are incorporated into the spliceosome. These events are prerequisite for formation of catalytically active spliceosome and normal pre-mRNA splicing (upper panel). OTS964 inhibits the ability of CDK11 to phosphorylate SF3B1 (dotted arrow) at the stage of B complex causing block of its transformation into the B^{act} complex and splicing defect (middle panel). In contrast, pladi B forces SF3B1 to remain in "open" conformation on BS adenosine, stalling spliceosome in A-like complex with outcome on splicing essentially the same as after the OTS964 treatment (lower panel). Black box=exon, black line=intron, 5´and 3´marks 5´ and 3´ ends of the transcript, respectively.

e, Working model: Outcome of splicing inhibition on transcription and RNAPII CTD phosphorylation. Inhibition of splicing by inhibitors targeting SF3B1 and spliceosome assembly (OTS964, pladi B) results in suboptimal transcription, likely affecting promoter-proximal pausing, elongation, and termination and in relatively unspecific bulk dephosphorylation of Tyr1 (Y1), Ser2 (S2), Thr4 (T4), Ser5 (S5) and Ser7(S7) in the CTD of RNAPII.

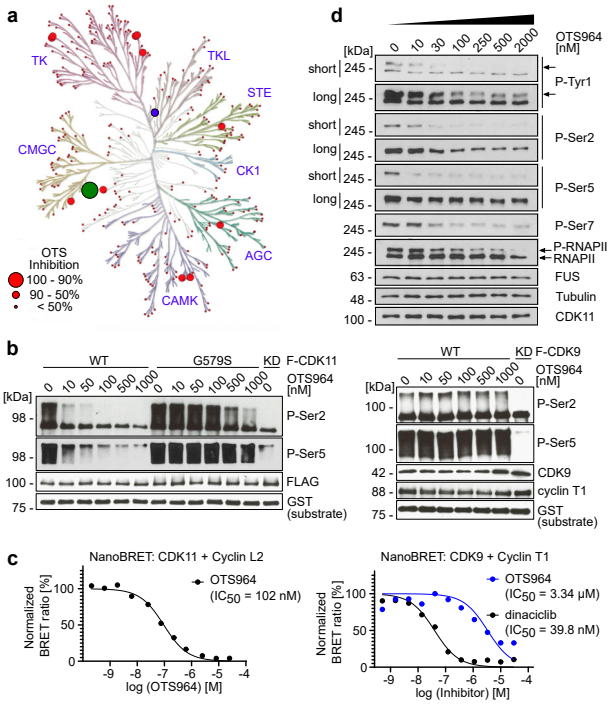
a
TK
TKL
STE
CMGC
CK1
AGC
CAMK
OTS
Inhibition
100 - 90%
90 - 50%
< 50%
d
[kDa]
0 10 30 100 250 500 2000
OTS964
[nM]
short
long
245 -
P-Tyr1
P-Ser2
P-Ser5
P-Ser7
P-RNAPII
RNAPII
63 -
FUS
48 -
Tubulin
100 -
CDK11
b
WT
G579S
KD
F-CDK11
0 10 50 100 500 1000 0 10 50 100 500 1000 0
OTS964
[nM]
[kDa]
98 -
P-Ser2
P-Ser5
100 -
FLAG
75 -
GST
(substrate)
WT
KD
F-CDK9
0 10 50 100 500 1000 0
OTS964
[nM]
[kDa]
100 -
P-Ser2
P-Ser5
42 -
CDK9
88 -
cyclin T1
75 -
GST
(substrate)
c
NanoBRET: CDK11 + Cyclin L2
Normalized
BRET ratio [%]
100
50
0
OTS964
(IC50 = 102 nM)
-9 -8 -7 -6 -5 -4
log (OTS964) [M]
NanoBRET: CDK9 + Cyclin T1
Normalized
BRET ratio [%]
100
50
0
OTS964
(IC50 = 3.34 µM)
dinaciclib
(IC50 = 39.8 nM)
-9 -8 -7 -6 -5 -4
log (Inhibitor) [M]

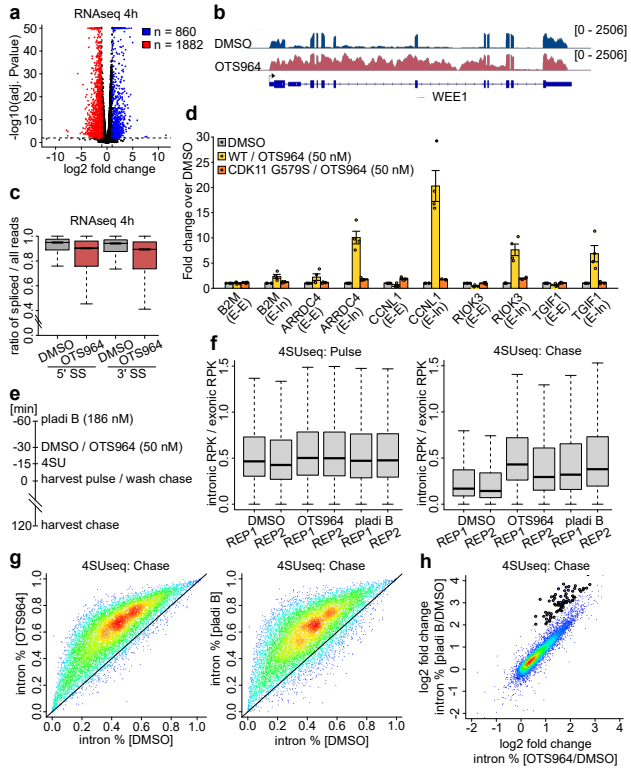
a
RNAseq 4h
n = 860
n = 1882
-log10(adj. Pvalue)
log2 fold change
b
DMSO
OTS964
[0 - 2506]
[0 - 2506]
WEE1
c
RNAseq 4h
ratio of spliced / all reads
DMSO
OTS964
DMSO
OTS964
5' SS
3' SS
d
DMSO
WT / OTS964 (50 nM)
CDK11 G579S / OTS964 (50 nM)
Fold change over DMSO
B2M (E-E)
B2M (E-In)
ARRDC4 (E-E)
ARRDC4 (E-In)
CCNL1 (E-E)
CCNL1 (E-In)
RIOK3 (E-E)
RIOK3 (E-In)
TGIF1 (E-E)
TGIF1 (E-In)
e
[min]
-60 pladi B (186 nM)
-30 DMSO / OTS964 (50 nM)
-15 4SU
0 harvest pulse / wash chase
120 harvest chase
f
4SUseq: Pulse
4SUseq: Chase
intronic RPK / exonic RPK
DMSO
OTS964
pladi B
REP1
REP2
g
4SUseq: Chase
4SUseq: Chase
intron % [OTS964]
intron % [pladi B]
intron % [DMSO]
h
4SUseq: Chase
log2 fold change intron % [pladi B/DMSO]
log2 fold change intron % [OTS964/DMSO]

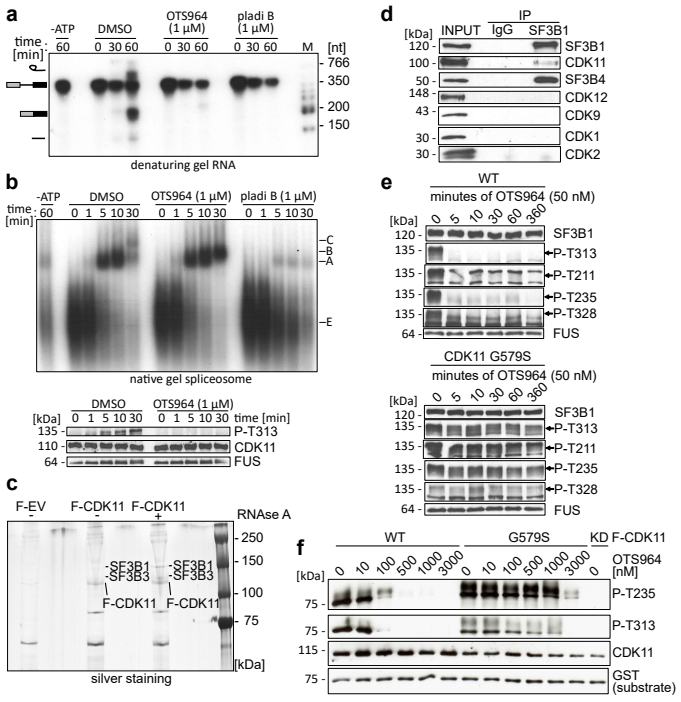
a
-ATP
DMSO
OTS964 (1 μM)
pladi B (1 μM)
time [min]
60
0 30 60
0 30 60
0 30 60
M
[nt]
766
350
200
150
denaturing gel RNA
b
-ATP
DMSO
OTS964 (1 μM)
pladi B (1 μM)
time [min]
60
0 1 5 10 30
0 1 5 10 30
0 1 5 10 30
C
B
A
E
native gel spliceosome
DMSO
OTS964 (1 μM)
[kDa]
0 1 5 10 30
0 1 5 10 30
time [min]
135
P-T313
110
CDK11
64
FUS
c
F-EV
F-CDK11
F-CDK11
RNAse A
-
-
+
250
150
100
75
[kDa]
SF3B1
SF3B3
SF3B1
SF3B3
F-CDK11
F-CDK11
silver staining
d
IP
[kDa]
INPUT
IgG
SF3B1
120
SF3B1
100
CDK11
50
SF3B4
148
CDK12
43
CDK9
30
CDK1
30
CDK2
e
WT
minutes of OTS964 (50 nM)
[kDa]
0 5 10 30 60 360
120
SF3B1
135
P-T313
135
P-T211
135
P-T235
135
P-T328
64
FUS
CDK11 G579S
minutes of OTS964 (50 nM)
[kDa]
0 5 10 30 60 360
120
SF3B1
135
P-T313
135
P-T211
135
P-T235
135
P-T328
64
FUS
f
WT
G579S
KD F-CDK11
[kDa]
0 10 100 500 1000 3000 0 10 100 500 1000 3000 0
OTS964 [nM]
75
P-T235
75
P-T313
115
CDK11
75
GST (substrate)

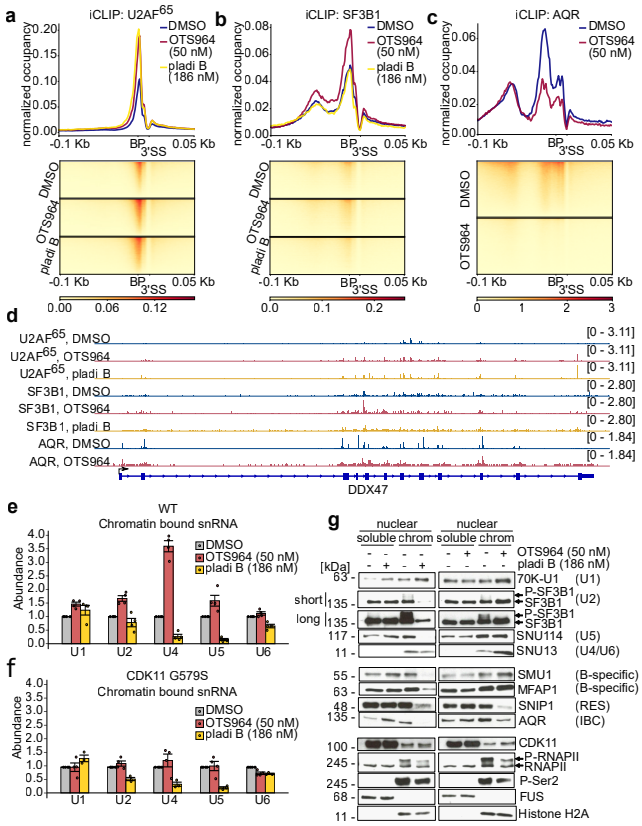
a
iCLIP: U2AF65
b
iCLIP: SF3B1
c
iCLIP: AQR
DMSO
OTS964 (50 nM)
pladi B (186 nM)
normalized occupancy
-0.1 Kb
BP
3'SS
0.05 Kb
d
U2AF65, DMSO
U2AF65, OTS964
U2AF65, pladi B
SF3B1, DMSO
SF3B1, OTS964
SF3B1, pladi B
AQR, DMSO
AQR, OTS964
[0 - 3.11]
[0 - 2.80]
[0 - 1.84]
DDX47
e
WT
Chromatin bound snRNA
Abundance
U1
U2
U4
U5
U6
f
CDK11 G579S
Chromatin bound snRNA
g
nuclear
soluble chrom
OTS964 (50 nM)
pladi B (186 nM)
[kDa]
70K-U1 (U1)
P-SF3B1
SF3B1 (U2)
short
long
SNU114 (U5)
SNU13 (U4/U6)
SMU1 (B-specific)
MFAP1 (B-specific)
SNIP1 (RES)
AQR (IBC)
CDK11
P-RNAPII
RNAPII
P-Ser2
FUS
Histone H2A